NAVAL POSTGRADUATE SCHOOL

MONTEREY, CALIFORNIA

THESIS

COOPERATIVE WIDEBAND SPECTRUM SENSING AND LOCALIZATION USING RADIO FREQUENCY SENSOR NETWORKS

by

Volkan Sönmezer

September 2009

Thesis Advisor:	Murali Tummala
Co-Advisor:	David Jenn

THIS PAGE INTENTIONALLY LEFT BLANK

REPORT DOCUMENTATION PAGE		*Form Approved OMB No. 0704-0188*
Public reporting burden for this collection of information is estimated to average 1 hour per response, including the time for reviewing instruction, searching existing data sources, gathering and maintaining the data needed, and completing and reviewing the collection of information. Send comments regarding this burden estimate or any other aspect of this collection of information, including suggestions for reducing this burden, to Washington headquarters Services, Directorate for Information Operations and Reports, 1215 Jefferson Davis Highway, Suite 1204, Arlington, VA 22202-4302, and to the Office of Management and Budget, Paperwork Reduction Project (0704-0188) Washington DC 20503.		
1. AGENCY USE ONLY *(Leave blank)*	**2. REPORT DATE** September 2009	**3. REPORT TYPE AND DATES COVERED** Master's Thesis
4. TITLE AND SUBTITLE Cooperative Wideband Spectrum Sensing and Localization Using Radio Frequency Sensor Networks		**5. FUNDING NUMBERS**
6. AUTHOR(S) Volkan Sönmezer		
7. PERFORMING ORGANIZATION NAME(S) AND ADDRESS(ES) Naval Postgraduate School Monterey, CA 93943-5000		**8. PERFORMING ORGANIZATION REPORT NUMBER**
9. SPONSORING /MONITORING AGENCY NAME(S) AND ADDRESS(ES) N/A		**10. SPONSORING/MONITORING AGENCY REPORT NUMBER**
11. SUPPLEMENTARY NOTES The views expressed in this thesis are those of the author and do not reflect the official policy or position of the Department of Defense or the U.S. Government.		
12a. DISTRIBUTION / AVAILABILITY STATEMENT Approved for public release; distribution is unlimited		**12b. DISTRIBUTION CODE**
13. ABSTRACT (maximum 200 words) This thesis implements spectrum sensing and localization tasks using a radio frequency sensor network and analyzes the performance of this implementation through simulation. A sensor network based cooperative wideband spectrum sensing and localization scheme is proposed for the implementation of the tasks. In the proposed scheme, wavelet-based multi-resolution spectrum sensing and received signal strength-based localization methods, which were originally proposed for cognitive radio applications, are adapted to radio frequency sensor networks. For cooperation of the nodes in the proposed scheme, a new three-bit hard combination technique is developed. A simulation model is created in MATLAB programming language to implement the proposed scheme and to analyze its simulation performance. The results of the simulation show that the proposed sensor network based cooperative wideband spectrum sensing and localization scheme is appropriate for radio frequency sensor networks and the proposed three-bit hard combination scheme is superior to the traditional hard combination schemes in terms of false alarm reduction.		
14. SUBJECT TERMS Cooperative Spectrum Sensing, Source Localization, Multi-Resolution Spectrum Sensing, Three-Bit Hard Combination, RSS-Based Localization, Cognitive Radio, Wireless Sensor Networks, Electronic Warfare		**15. NUMBER OF PAGES** 109
		16. PRICE CODE
17. SECURITY CLASSIFICATION OF REPORT Unclassified	**18. SECURITY CLASSIFICATION OF THIS PAGE** Unclassified	**19. SECURITY CLASSIFICATION OF ABSTRACT** Unclassified	**20. LIMITATION OF ABSTRACT** UU

i

THIS PAGE INTENTIONALLY LEFT BLANK

COOPERATIVE WIDEBAND SPECTRUM SENSING AND LOCALIZATION USING RADIO FREQUENCY SENSOR NETWORKS

Volkan Sönmezer
1st Lieutenant, Turkish Air Force
B.S., Gazi University, 2000

Submitted in partial fulfillment of the
requirements for the degrees of

**MASTER OF SCIENCE IN ELECTRONIC WARFARE
SYSTEMS ENGINEERING**
and
MASTER OF SCIENCE IN ELECTRICAL ENGINEERING

from the

**NAVAL POSTGRADUATE SCHOOL
September 2009**

Author: Volkan Sönmezer

Approved by: Murali Tummala
                Thesis Advisor

                David Jenn
                Thesis Co-Advisor

                Dan C. Boger
                Chairman, Department of Information Sciences

                Jeffrey B. Knorr
                Chairman, Department of Electrical and Computer Engineering

iii

THIS PAGE INTENTIONALLY LEFT BLANK

ABSTRACT

This thesis implements spectrum sensing and localization tasks using a radio frequency sensor network and analyzes the performance of this implementation through simulation. A sensor network based cooperative wideband spectrum sensing and localization scheme is proposed for the implementation of the tasks. In the proposed scheme, wavelet-based multi-resolution spectrum sensing and received signal strength-based localization methods, which were originally proposed for cognitive radio applications, are adapted to radio frequency sensor networks. For cooperation of the nodes in the proposed scheme, a new three-bit hard combination technique is developed. A simulation model is created in MATLAB programming language to implement the proposed scheme and to analyze its simulation performance. The results of the simulation show that the proposed sensor network based cooperative wideband spectrum sensing and localization scheme is appropriate for radio frequency sensor networks and the proposed three-bit hard combination scheme is superior to the traditional hard combination schemes in terms of false alarm reduction.

THIS PAGE INTENTIONALLY LEFT BLANK

TABLE OF CONTENTS

LIST OF FIGURES

x

LIST OF TABLES

THIS PAGE INTENTIONALLY LEFT BLANK

EXECUTIVE SUMMARY

Spectrum sensing and localization are two important tasks in electronic warfare, signal intelligence and cognitive radios. In electronic warfare and signal intelligence, these tasks can be implemented using a radio frequency sensor network to detect the signals in the air, determine their frequencies, and estimate the locations and effective isotropic radiated powers (EIRPs) of the radio frequency sources emitting the signals of interest. In cognitive radios, unlicensed users implement spectrum sensing and localization not to interfere with licensed users. Cooperation in spectrum sensing and localization improves the signal detection and position estimation performance under fading, shadowing or noisy conditions.

The objective of this thesis is to implement collaborative spectrum sensing and localization using a radio frequency sensor network. In particular, the aim is to determine the frequencies of the signals in the air, and estimate the locations and EIRPs of the sources emitting these signals through collaborations of the sensor nodes. An additional objective is to minimize the computational complexity and maximize the sensing and localization performance. To achieve these objectives, a sensor network based cooperative wideband spectrum sensing and localization scheme is proposed. This scheme uses a wavelet-based multi-resolution spectrum sensing (MRSS) method for spectrum sensing, a new three-bit hard combination technique for collaboration, and a received signal strength (RSS)-based localization method for location and EIRP estimation. MRSS and RSS-based localization methods, which were originally proposed for cognitive radio applications in the literature, are adapted to RF sensor networks in this thesis.

A simulation model was developed in MATLAB programming language to implement the proposed scheme and to analyze its simulation performance. In the performance analysis of the cooperative wideband spectrum sensing part of the proposed scheme, the effects of different window types, number of power spectral densities (PSDs) averaged, number of nodes, signal-to-noise-ratio (SNR) values, and number of

transmitters on the detection performance were simulated. Performance of a new three-bit hard combination scheme was compared with traditional hard combination schemes. Different values of the number of samples, number of nodes, and standard deviation of the Gaussian variable in the shadowing model were simulated to determine their effects on the performance of the localization part of the proposed scheme.

The results of the simulations showed that the proposed sensor network based cooperative wideband spectrum sensing and localization scheme is appropriate for radio frequency sensor networks. Redundant, exhaustive sensing on empty bands is avoided with MRSS, and less overhead in collaboration with respect to the soft combination is provided by three-bit hard combination. RSS-based localization scheme not only estimates the location of the signal of interest sources, but also their EIRP. Cooperation of the nodes provides resilience to fading, shadowing, and noise.

Another result of the simulation is that the proposed three-bit hard combination scheme is superior to the traditional hard combination schemes in false alarm reduction, and the detection performance of the three-bit combination scheme can be improved with little additional cost by increasing the number of averaged PSDs.

The simulation results also showed that for the localization part of the proposed scheme, average absolute power estimation error presents the same behavior as the position estimation mean squared error. In particular, the number of samples, number of nodes, and standard deviation of the Gaussian variable in the shadowing model affect both error metrics in a similar manner.

ACKNOWLEDGMENTS

THIS PAGE INTENTIONALLY LEFT BLANK

I.   INTRODUCTION

Wireless sensor networks, consisting of a large number of randomly deployed, low-cost, low-power, multifunctional nodes collaborating to achieve a common goal, are used in a variety of applications including military [1]. By being equipped with appropriate sensors, these networks can detect, identify and analyze sensor signal data to monitor enemy activity [2]. In particular, a wireless network consisting of radio frequency (RF) sensor nodes can be used to implement electronic warfare (EW) tasks, such as spectrum sensing and localization.

A wireless sensor network consisting of RF sensor nodes that are deployed within an area of interest can be used to detect the signals in the air, to determine their frequencies, and to estimate the locations and effective isotropic radiated powers (EIRPs) of the RF sources emitting these signals. Figure 1 depicts a scenario for this purpose. The collaboration among the sensor nodes not only improves the detection performance and estimation accuracy but also increases the life of the sensor nodes by decreasing the detection time required [3].

Spectrum sensing and localization are also implemented in cognitive radios, which can be defined as smart radios having the ability to be aware of the electromagnetic environment. Secondary users, also called unlicensed users, implement spectrum sensing and sometimes localization to use the licensed spectrum bands without interfering with the primary users having priority of service [3]. In particular, secondary users utilize spectrum sensing to find unoccupied frequency bands where communication is possible. As in RF sensor networks, cooperation in spectrum sensing and localization improves the performance of cognitive radio networks.

Due to the two important application areas briefly mentioned above, namely EW and cognitive radio, spectrum sensing and localization are active research topics. Many researchers work on spectrum sensing and localization methods to improve the efficiency and performance of these methods.
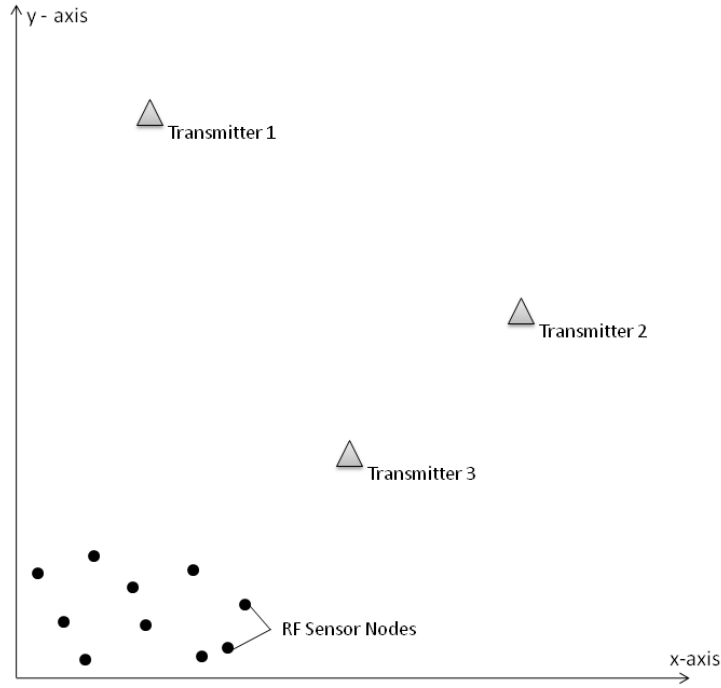
Figure 1.   A Scenario of Using a RF Sensor Network to Determine the Frequency Bands, Locations and EIRPs of the Source Transmitters.

A.   THESIS OBJECTIVE

The objective of this thesis is to implement collaborative spectrum sensing and localization of RF sources using a sensor network as an EW task. Figure 1 shows the EW scenario adopted in this thesis. The purpose of the RF sensor network is to determine the frequencies of the RF sources and to estimate the location and EIRP of these transmitters. An additional objective is to minimize the computations needed for spectrum sensing and source localization, while maximizing the signal detection performance and accuracy of the estimations of the transmitters' location and EIRP. When the limited battery energy of each node is taken into consideration, the importance of this objective is easily understood.

A sensor network based cooperative wideband spectrum sensing and localization scheme is proposed in this thesis to achieve these objectives. This proposed scheme uses

2

a wavelet-based multi-resolution spectrum sensing (MRSS) method [4] for spectrum sensing, a new three-bit hard combination technique for collaboration, and received signal strength (RSS)-based localization method [5] for localization. MRSS and RSS-based localization methods were originally proposed for cognitive radio applications in the literature and are adapted to RF sensor networks in this thesis.

A simulation model will be developed in MATLAB programming language to implement the proposed scheme and to analyze its simulation performance.

B.   RELATED WORK

Spectrum sensing and cooperation in spectrum sensing are currently two of the most active research topics in wireless communications. This popularity is due to emerging cognitive radio applications. Much of the spectrum sensing work in the literature has been concerned with cooperative spectrum sensing in cognitive radios. Hur et al. [4] studied wavelet-based MRSS for cognitive radios. Ma et al. [6] proposed a two-bit hard combination and detection scheme for spectrum sensing in cognitive radio networks.

Much has been written in the literature on emitter localization. Kim et al [5] studied RSS-based localization to find the position and EIRP of the primary users in cognitive radios.

This thesis will use the MRSS scheme from [4] for the spectrum sensing task and use ideas from [6] as a starting point for the proposed three-bit hard combination scheme. The source localization scheme used in the thesis is based on the work reported in [5].

C.   THESIS OUTLINE

The organization of this thesis is as follows. Chapter II covers the spectrum sensing methods, localization algorithms, and application areas of spectrum sensing and localization. Chapter III describes the proposed sensor network based cooperative wideband spectrum sensing and localization scheme and presents the fundamental techniques used in the scheme. In particular, the MRSS, cooperative spectrum sensing,

proposed three-bit hard combination scheme, and RSS-based localization scheme are discussed. Chapter IV describes the simulation model and presents the simulation results. Chapter V summarizes the thesis work, and highlights future work for further investigation. The Appendix presents selected MATLAB code developed as part of this work.

II.   BACKGROUND

As mentioned in Chapter I, spectrum sensing and localization are two important functions used in electronic warfare (EW) and cognitive radio applications. This chapter presents background on spectrum sensing and source localization. Firstly, three important spectrum sensing methods are discussed; then localization algorithms are briefly mentioned. Application areas of spectrum sensing and localization, namely electronic warfare and cognitive radio, are also described.

A.   SPECTRUM SENSING METHODS

Spectrum sensing can be defined as examining the radio spectrum to determine the used or unused frequency bands. In EW applications, it is used to find the occupied frequency bands in the spectrum, whereas in cognitive radio, it is applied to detect the unoccupied frequency bands to communicate.

This section discusses the three most common spectrum sensing methods reported in the literature.

1.   Energy Detector-based Sensing

Energy detector-based sensing is one of the most common sensing methods [7]. It uses the energy of the received signal to decide on the presence of the signal. Figure 2 shows an implementation of this method. As seen in this figure, the received signal of interest is filtered, converted to a digital form, squared and integrated over the observation interval to obtain the signal energy [8]. This energy is compared with a threshold to decide on the presence of the signal of interest [8].

Energy detector-based sensing, also known as radiometry, is the optimal spectrum sensing method, when the information about the signal of interest is not known [8]. It is easy to implement and has low computational complexity [7].

Since the received energy is compared to a threshold in energy detector-based sensing, the threshold selection affects the performance of the method significantly. This

method is also susceptible to uncertainty in the noise power [8]. At low signal-to-noise ratio (SNR) values, from -10 dB to -40 dB, this detector requires more detection time compared to the matched filtering method detector [8] presented in Chapter II.A.3.

In this thesis, multi-resolution spectrum sensing, an improved energy detector based sensing method [9], is used.
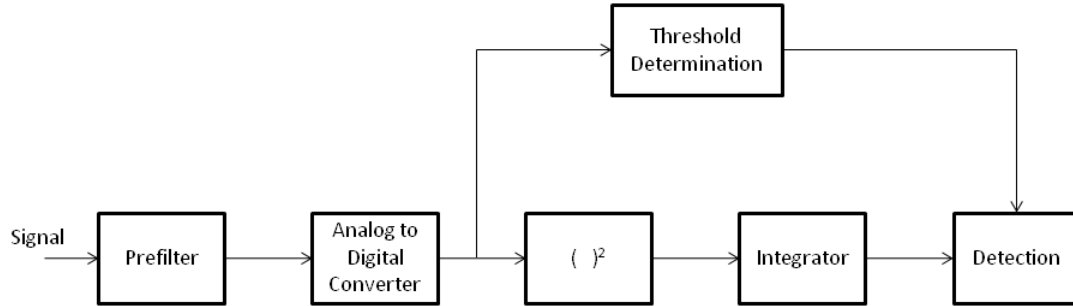
Figure 2.   An Implementation of Energy Detector-based Sensing (After [10]).

2.   Cyclostationary-based Sensing

In the cyclostationary-based sensing method, cyclostationary features of the modulated signals are exploited. Cyclostationary features are the inherent results of the periodic structures of the modulated signals, such as sinusoidal carriers, pulse trains, hopping sequences, or cyclic prefixes [8]. Due to this built-in periodicity, modulated signals are cyclostationary with spectral correlation [8].

Figure 3 shows an implementation of the cyclostationary-based sensing method. As seen in this figure, first the spectral components of the input signal are computed through the fast Fourier transform (FFT) [10]. Then the spectral correlation is performed on these spectral components and the spectral correlation function is estimated [10]. This spectral correlation function is analyzed to detect the signals in the cyclostationary-based spectrum sensing method [8].

The biggest advantage of this method is that it is robust to uncertainty in noise power [8]. This robustness comes from the fact that the noise is a wide-sense stationary process with no spectral correlation, whereas the modulated signals are cyclostationary with spectral correlation [8].

On the other hand, cyclostationary-based sensing has increased computational complexity and requires longer observation time than the energy detector-based sensing schemes [8].
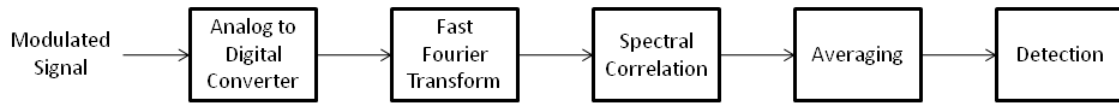
Figure 3.   An Implementation of Cyclostationary-based Sensing (After [10]).

3.   Matched Filtering

Matched filtering is a spectrum sensing method that uses a priori knowledge of the characteristics of the received signal [8]. This a priori knowledge may include modulation type and order, pulse shaping, packet format, bandwidth, frequency, etc. [7, 10]. Figure 4 shows an implementation of the matched filtering method. In this figure, "pilot" is a priori knowledge of the signal of interest. The pilot is correlated to the received signal and then compared to a threshold for detection. In the matched filtering method, the receiver has to achieve coherency with the input signal by using timing and carrier synchronization [10].

Matched filtering is the optimal spectrum sensing method when the information about the signal of interest is known [7]. To achieve a certain probability of false alarm, this method requires shorter time as compared to the energy detector-based sensing and cyclostationary-based sensing methods [7].

7

The need for a priori knowledge is the main disadvantage of the matched filtering method [7]. The requirement of synchronization between the transmitter and the receiver is another disadvantage of this method [8]. Moreover, if a variety of signal types must be received, complexity of this implementation is high [7].
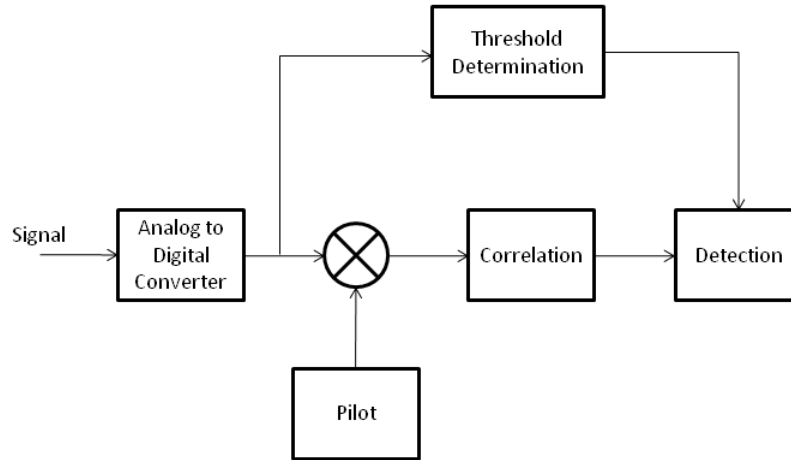
Figure 4.   An Implementation of the Matched Filtering Method (After [10]).

B.   LOCALIZATION SCHEMES

The localization operation is used to determine the position of the source of the signal of interest. In an EW application, it is used to determine the location of an adversary's transmitter, whereas in a cognitive radio, it is used to determine the location of a primary user. Localization schemes can be classified into two categories, namely, range-based localization schemes and range-free localization schemes [11]. This section discusses these two categories.

1.   Range-based Localization Schemes

Range-based localization schemes exploit ranging to estimate the location of the source. Range-based localization schemes use different metrics, such as time of arrival (TOA), time difference of arrival (TDOA), angle of arrival (AOA), or received signal strength (RSS) metrics.

TOA is found by measuring the time at which a radio frequency (RF) signal first arrives at a receiver [12]. The measured TOA is equal to the transmission time plus time delay due to propagation [12]. The distance information is found from the propagation delay between a source and a receiver [13].

In TDOA-based schemes, the difference of the TOAs in different receivers is used to estimate the location of a source [13]. This estimation can either use the difference in the times at which a single signal from the source arrives at three or more nodes, or the difference in the times at which multiple signals from the source arrive at one receiver [13]. Hence, in TDOA based schemes, highly precise synchronization between the receivers is required, but precise synchronization between source and receivers is not required [13].

In range-based localization schemes, based on an AOA metric, the distance between receivers is formed using the angle between them [13]. Adoption of antenna arrays and a minimum distance between the antenna elements are required in this scheme [13]. Another disadvantage is that this scheme is highly sensitive to multipath, non-line-of-sight conditions, and array precision [13].

RSS is the squared magnitude of the signal amplitude that is the measured power [12]. It is measured by a receiver's received signal strength indicator circuit [12]. In RSS-based localization schemes, the distance is measured based on the attenuation due to the propagation of the signal from source to receiver [13]. This localization scheme requires an accurate propagation model to estimate the distance reliably, since the channel affects the relation between distance and attenuation [13].   Since RSS measurements are relatively inexpensive and easy to implement, this scheme has low cost [12]. Some of the RSS-based localization schemes require knowledge of the effective

9

isotropic radiated power (EIRP) of the transmitter [5]. An example of an algorithm using the RSS metric without knowledge of EIRP of transmitter is given in [5].

2. Range-free Localization Schemes

Range-free localization schemes are used to find the node positions in wireless networks. Anchor nodes, with known coordinates, are deployed across the wireless network and sensor positions are found from the estimated distance to multiple anchors and their coordinates [14]. In particular, the information of anchor nodes or the connectivity of the wireless network is exploited to estimate the position of the transmitter [11]. Each anchor may have a Global Positioning System (GPS) receiver to find its position [15]. Since the nodes do not need extra hardware for providing range information, range-free localization schemes are more cost effective than range-based localization schemes [14].

C. APPLICATION AREAS OF SPECTRUM SENSING AND LOCALIZATION

EW, which has been an important topic since the 1960s, is an inseparable part of today's military operations and uses spectrum sensing and localization extensively. Cognitive radio, an emerging communication technology, first proposed in 1999, exploits spectrum sensing and localization for its operation. This section describes cognitive radio and EW concepts in addition to signals intelligence (SIGINT).

1. Cognitive Radio

Cognitive radio is an emerging technology [16] in which one of the intents is to use the frequency spectrum efficiently.

A cognitive radio is a smart radio that knows where it is, what services are available, what services interest the user, and how to find these interested services [17]. It also knows the current and future, communication and computing needs of its user [17]. One of its objectives is to find and use the empty spectral band to communicate more efficiently [17].

The definition of the cognitive radio according to the Software Defined Radio (SDR) Forum is given as [18]

a) Radio in which communication systems are aware of their environment and internal state and can make decisions about their radio operating behavior based on that information and predefined objectives. The environmental information may or may not include location information related to communication systems.

b) Cognitive Radio (as defined in a) that utilizes Software Defined Radio, Adaptive Radio, and other technologies to automatically adjust its behavior or operations to achieve desired objectives.

A cognitive radio is aware of its physical, operational and electromagnetic environments [19]. Position in space, proximity to various networks, and knowledge of the weather conditions are examples of the physical environment aspects of which a cognitive radio can be aware [19]. Awareness in the operational environments may include a user's usage pattern and operating preferences [19]. Signals in the air form the local radio spectrum, which means electromagnetic environment. The ability of a cognitive radio in becoming aware of signals in the local spectrum is called spectrum sensing in cognitive radio [19].

In a cognitive radio system, users having the priority to use the spectrum are called primary users, whereas the users that use the unoccupied bands not used by primary users are called secondary users. Secondary users apply spectrum sensing to find these unoccupied radio frequency bands that can be used for communication. Therefore, spectrum sensing is one of the key functions of a cognitive radio system's operation.

Location information related to communication systems is also considered in the above definition of cognitive radio given by the SDR Forum. Location information of the primary users can be useful for transmission between secondary users [20]. Localization can be used to track the primary users or to assist the transmission between secondary users [20]. For example, secondary users can be allocated at a distance where they detect the presence of a primary signal well outside the primary user's transmission coverage [3].

In summary, it can be said that efficient implementation of spectrum sensing and localization is essential for cognitive radio operation.

2. Electronic Warfare and Signal Intelligence

The objective of electronic warfare (EW) is to command the electromagnetic spectrum with electronic attack (EA), electronic protection (EP), and electronic warfare support (ES) actions [21]. ES, formerly known as electronic support measures (ESM), supplies the intelligence and threat recognition that allow the implementation of EA and EP [21]. ES involves the act of intercepting, identifying, analyzing and locating an enemy's radiations [21]. Thus spectrum sensing and localization are two important actions in ES. Finding the frequency of the enemy signal and location of the enemy transmitter assists the EA and EP actions.

Collecting, analyzing, identifying and locating the emitter signals of the enemy are also used for SIGINT. SIGINT has two components: communications intelligence (COMINT) and electronic intelligence (ELINT). COMINT is used against enemy communication signals, whereas ELINT is used against enemy noncommunication signals, such as radar signals [21]. Both COMINT and ELINT use spectrum sensing and localization to gather intelligence about the enemy communication transmitters or radars.

It can be concluded that spectrum sensing, which can be used to identify the frequency of the enemy signal, and localization, which can be used to locate the enemy transmitters, are the core actions in EW and SIGINT.

D. SUMMARY

In this chapter, the most common spectrum sensing methods and localization algorithms were briefly discussed. Application areas of spectrum sensing and localization were also mentioned. The next chapter will discuss the proposed sensor network based cooperative wideband spectrum sensing and localization scheme and the fundamental concepts used in this scheme.

III. COOPERATIVE WIDEBAND SPECTRUM SENSING AND LOCALIZATION SCHEME USING RADIO FREQUENCY SENSOR NETWORKS

As mentioned in Chapter I, a radio frequency (RF) sensor network can be used to detect the signals in the air, to determine their spectral bands, and to estimate the locations and effective isotropic radiated powers (EIRPs) of the transmitters emitting these signals. It was also mentioned that minimizing the computational load in this network while maximizing the detection performance and estimation accuracy is also desirable.

This chapter presents the proposed sensor network based cooperative wideband spectrum sensing and localization scheme to achieve the above objectives. Fundamental concepts used in this scheme are also described. In particular, multi-resolution spectrum sensing, cooperation in spectrum sensing, a new three-bit hard combination scheme and a received signal strength based localization technique are discussed.

A.   PROPOSED SENSOR NETWORK BASED COOPERATIVE WIDEBAND SPECTRUM SENSING AND LOCALIZATION SCHEME

Figure 5 shows a functional block diagram of the sensor network based cooperative wideband spectrum sensing and localization scheme proposed in this thesis. The function of each block is as follows. All nodes in the RF sensor network apply coarse resolution sensing to obtain a quick examination of the spectrum of interest. Three-bit hard combination combines the coarse resolution sensing results to detect the signals in the air and to determine the frequency bands that need to be exhaustively inspected. Fine resolution sensing is applied to these frequency bands to narrow down the spectral bands of the signals in the air. Specific techniques used for received signal strength (RSS) measurement at the nodes and the calculation of the relative node positions are not presented in this thesis and assumed to be made available. The function of the localization block is to estimate the position and EIRP of the transmitters emitting these signals, given the RSS and relative node position values.
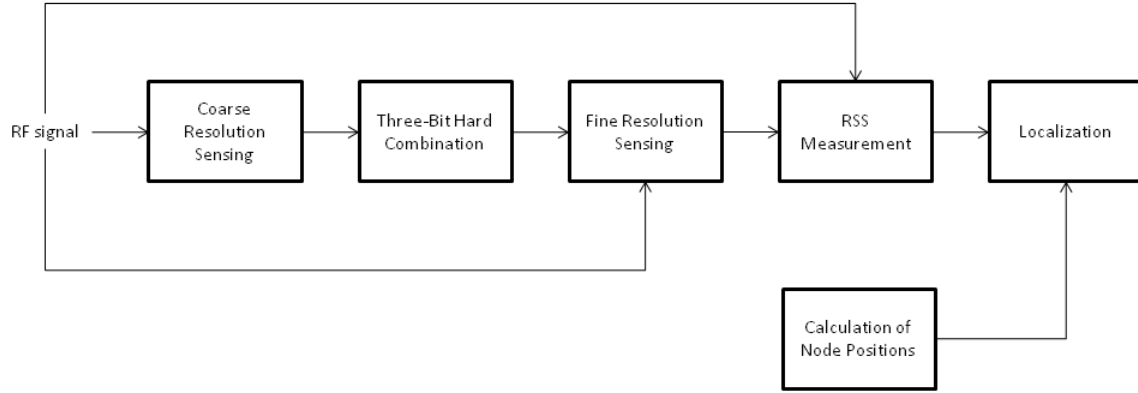
Figure 5.   Functional Block Diagram of the Proposed Sensor Network Based
Cooperative Wideband Spectrum Sensing and Localization Scheme.

This proposed sensor network based cooperative wideband spectrum sensing and localization scheme uses a wavelet-based multi-resolution spectrum sensing (MRSS) technique [4] in the coarse and fine resolution sensing blocks, a proposed three-bit hard combination scheme in the three-bit hard combination block, and a RSS-based localization technique [5] in the localization block.   A discussion of the scheme's algorithm follows.

Firstly, a node designated as the decision maker applies coarse resolution spectrum sensing to the entire bandwidth of interest and determines seven thresholds, which are used to divide the observation range into eight regions, as explained in Chapter III.C.3. All other nodes are informed of these threshold values so that every node is able to apply the same thresholds. Then, all nodes, except for the decision maker node, apply coarse resolution spectrum sensing to the entire bandwidth of interest. After applying the thresholds, the nodes evaluate those frequency bands in which sensed energy exceeds the first threshold and determine the region of the sensed energy.   Then, nodes send information about the observed energy regions as three-bit values to the decision maker. The decision maker determines the spectrum bands on which fine resolution spectrum sensing will be applied by using the proposed three-bit hard combination scheme. The decision maker also decides which nodes will apply fine resolution spectrum sensing on

the determined spectrum bands. In particular, nodes that sense the highest energies on the determined spectrum bands apply fine resolution sensing. After fine resolution sensing is applied at each selected node, each of the nodes applies the maximum of the seven threshold values that is below the maximum observed energy sensed by coarse resolution sensing in the determined spectrum band. In this way, selected nodes determine the frequency bands of the signals in the air.

For finding the locations of the transmitters, the decision maker uses the averaged RSS values from the nodes and the positions of the nodes, and then applies the RSS-based localization scheme explained in Chapter III.D.

The following sections provide a detailed explanation of the techniques used in the proposed sensor network based cooperative wideband spectrum sensing and localization scheme.

B.   MULTI-RESOLUTION SPECTRUM SENSING

MRSS is a kind of energy detector [9]. The basis for MRSS is the sensing of a spectrum at two different resolutions: coarse resolution and fine resolution. In MRSS techniques, coarse resolution spectrum sensing is applied to the entire bandwidth of the system [22]. This provides a quick examination of the spectrum of interest. Then, fine resolution sensing is performed on the spectral bands in which further inspection is necessary [22]. With this method, the entire bandwidth of the system is not examined exhaustively; therefore, sensing time and power consumption are reduced significantly [22].

In the literature only a few applications of the MRSS technique [4], [22], [23] are documented. These techniques are classified as either wavelet-based or fast Fourier transform (FFT)-based approaches.

The following subsections discuss both of these approaches. The wavelet-based MRSS technique is explained in greater detail since it is used in the proposed sensor network based cooperative wideband spectrum sensing and localization scheme. The FFT-based MRSS technique is presented for completeness.

15

1.   Wavelet-based MRSS

Figure 6 shows the functional block diagram of a wideband analog wavelet-based MRSS technique proposed in [4].   In this wavelet-based MRSS technique, the pulse duration of the wavelet generator and frequencies of the sinusoidal functions are changed to sense the spectrum with different resolutions [4].   In particular, to obtain different sensing resolutions, wavelet pulse width T_g and frequency increment f_{sweep} are adjusted [9], and to scan the frequency band of interest, inspected frequency value f_k is changed. The use of a large T_g or a smaller f_{sweep} provides fine resolution sensing, whereas the use of a smaller T_g or a large f_{sweep} provides coarse resolution sensing.   As shown in Figure 6, first, a wavelet pulse with duration T_g is multiplied by a cosine and sine functions having the same frequency as the inspected frequency.   Then, the results of these multiplications are multiplied by the received RF signal.   After that, integration and digitization are applied in the analog correlators.   The outputs of the analog correlators are first squared and then summed. The square root of this sum gives the spectral density at f_k [4]. The detailed explanation of this operation follows.
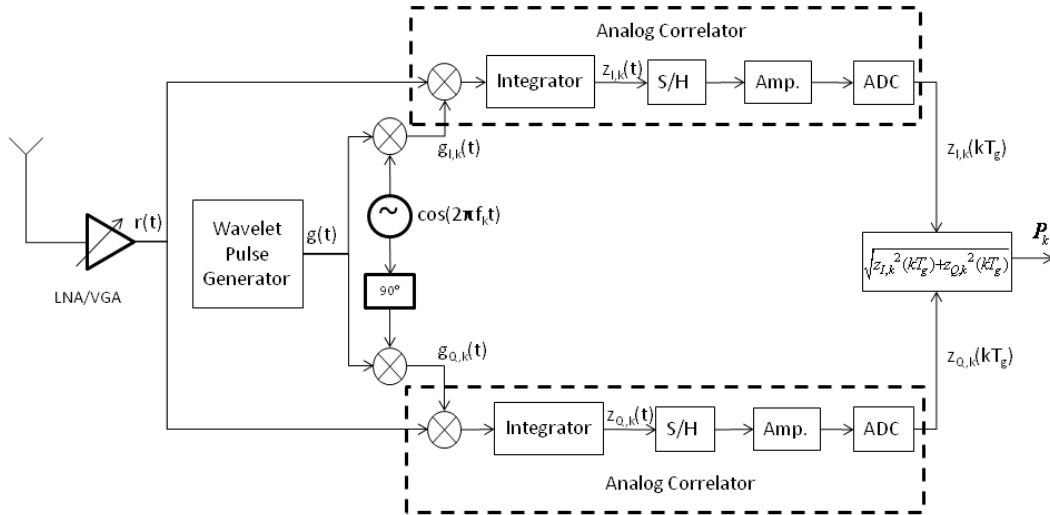
Figure 6.   Functional Block Diagram of Wavelet-based MRSS (From [24]).

16

In Figure 6, $g_{I,k}(t)$ and $g_{Q,k}(t)$ are given by [4]

$$g_{I,k}(t) = g(t)\cos(2\pi f_k t) \qquad \text{for } k = 0,...,K$$

$$g_{Q,k}(t) = g(t)\sin(2\pi f_k t) \qquad \text{for } k = 0,...,K$$

where $g(t)$ is a wavelet pulse, $f_k = (f_{\text{start}} + kf_{\text{sweep}})$ is the kth inspected frequency value and $K = \text{Round}[(f_{\text{stop}} - f_{\text{start}})/f_{\text{sweep}}]$ is the number of inspected frequency values.

The frequency interval $(f_{\text{stop}} - f_{\text{start}})$ is examined by changing f_k by the amount of f_{sweep} [4]. The spectral contents $z_{I,k}(t)$ and $z_{Q,k}(t)$ of input signal $r(t)$ are calculated by analog correlators for every f_k, which are equal to [4]

$$z_{I,k}(t) = \frac{1}{T_g}\int_{k\cdot T_g}^{(k+1)\cdot T_g}\Big[r(t)\big\{g(t)\cos(2\pi f_k t)\big\}\Big]dt$$

$$z_{Q,k}(t) = \frac{1}{T_g}\int_{k\cdot T_g}^{(k+1)\cdot T_g}\Big[r(t)\big\{g(t)\sin(2\pi f_k t)\big\}\Big]dt$$

The magnitude P_k represents the spectral density at frequency f_k and is given by [4]

$$P_k = \sqrt{z_{I,k}{}^2(kT_g) + z_{Q,k}{}^2(kT_g)}$$

where $z_{I,k}(kT_g)$ and $z_{Q,k}(kT_g)$ are the discrete values of $z_{I,k}(t)$ and $z_{Q,k}(t)$, which are obtained by sampling at every wavelet pulse width T_g.

Averaging is considered to improve the spectral density estimation performance of this technique [4]. In particular, P_k is calculated more than once and the results are averaged. Averaging reduces the noise floor level and makes the signals' spectra more discernable [4].

Coarse resolution sensing and fine resolution sensing concepts can be better understood by an examination of the results of this technique presented in [4]. Figure 7 shows the spectrum of an input RF signal to the system shown in Figure 6. In Figure 7,

17

there are three signals in the medium having carrier frequencies: 597 MHz, 615 MHz and 633 MHz, with bandwidths: 200 kHz, 6 MHz and 7 MHz, respectively.
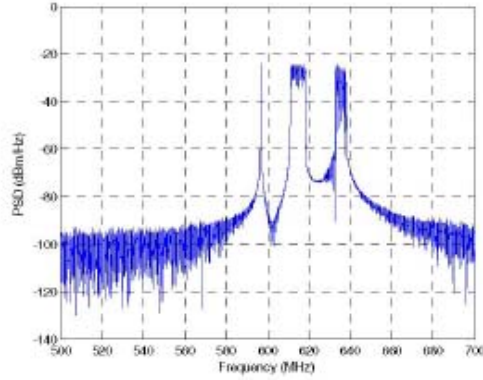
Figure 7.   Spectrum of an Input RF Signal for the System Shown in Figure 6 (From [4]).

Figure 8 shows the result of coarse resolution spectrum sensing with a window pulse width T_g of 0.1 μs and a frequency increment f_{sweep} of 5 MHz. Figure 9 shows the result of fine resolution spectrum sensing with a window pulse width T_g of 1 μs and a frequency increment f_{sweep} of 2 MHz. Window pulse width T_g and frequency increment f_{sweep} determine the resolution of this scheme. Note that the lower the f_{sweep} value and the higher the T_g value, the higher the sensing resolution. By comparing Figure 8 and Figure 9, sharp peaks for each input signal in Figure 9 show that fine resolution sensing gives better detection performance in terms of sensing resolution [4].
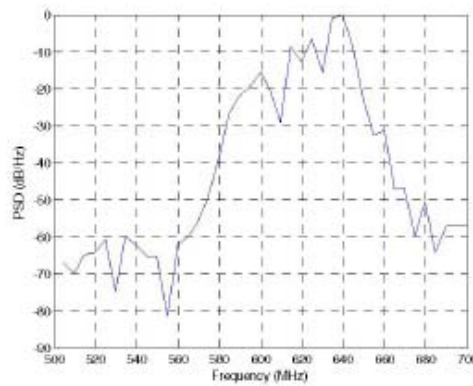
Figure 8.   Coarse Resolution Sensing Result with $T_g = 0.1\,\mu s$, $f_{sweep} = 5\,MHz$ (From [4]).

18
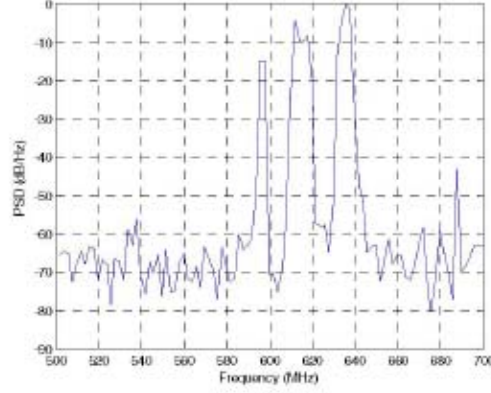
Figure 9.   Fine Resolution Sensing Result with $T_g = 1\,\mu s$, $f_{sweep} = 2\,\text{MHz}$ (From [4]).

One of the advantages of this technique is that a wavelet pulse acts as a bandpass filter and rejects the noise in the input RF signal [4]. Since the resolution is adjusted by changing the wavelet pulse width T_g and the frequency increment f_{sweep}, a filter bank or tunable filter is not needed [25]. Moreover, since most of the computation is done in the analog domain, digital circuit complexity can be significantly reduced [25] and low-power and real-time operations are realizable [4].

2.   FFT-based MRSS

In FFT-based MRSS techniques, the size of the FFT that produces the spectrum is changed to implement coarse and fine resolution sensing. For coarse resolution sensing, a small size FFT is used, and for fine resolution sensing a larger size FFT is used. Two implementations of FFT-based MRSS techniques are proposed in [23] and [22].

Figure 10 and Figure 11 show the block diagrams of the coarse and fine resolution modes of the MRSS technique for an M_{Ant} - antenna receiver as proposed in [23]. As can be seen from these block diagrams, a larger size FFT is used for fine resolution sensing. Since parallel sensing is applied in addition to MRSS, more than one antenna is used in this technique. Parallel sensing provides a reduced total sensing time [23].

As seen in Figure 10, for coarse resolution sensing, a multitone frequency generator generates different center frequencies that will be sensed. Down-converted

19

frequency bands are digitized and fed into N_{FFT}/M_{Ant} point FFT blocks [23]. Then, the outputs of the FFT blocks are used by the sensing block to determine the energies in the respective frequency bands [23]. After this process, the medium access control block requests the multitone frequency generator to generate another set of center frequencies, and sensing is repeated until the whole bandwidth of interest has been scanned [23].
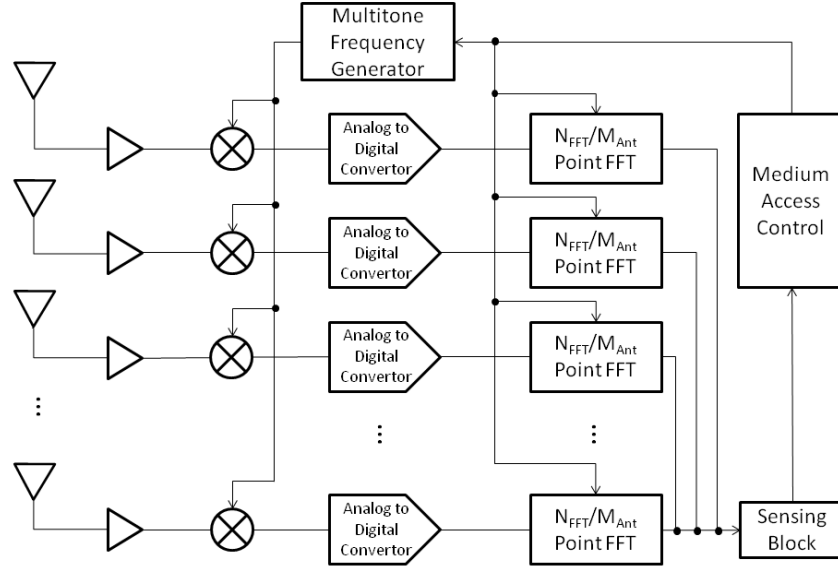
Figure 10.   Block Diagram of the Coarse Resolution Sensing Mode (From [23]).
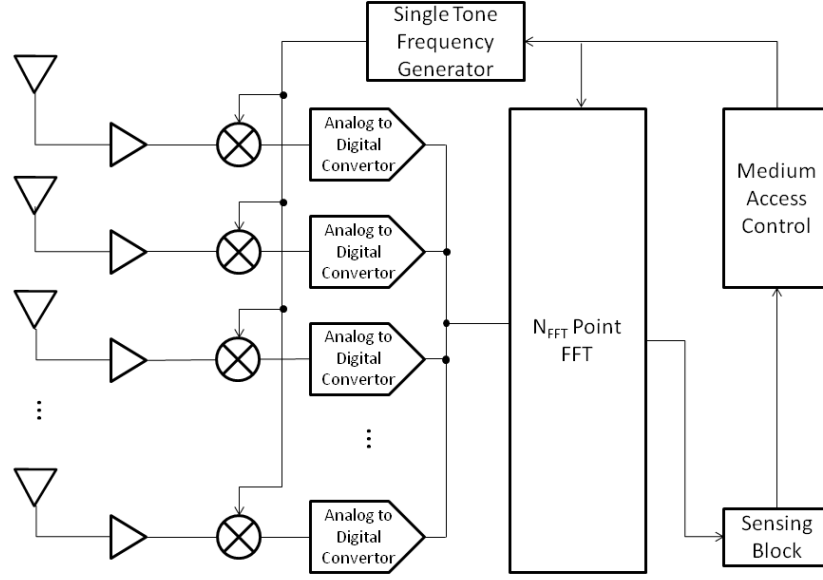
Figure 11.   Block Diagram of the Fine Resolution Sensing Mode (From [23]).

As depicted in Figure 11, in fine resolution sensing, signals having the same frequency value, as determined by the single tone frequency generator, are down-converted, digitized and input to a N_{FFT} point FFT. Then, the output of the FFT block is used to determine the energy content of the single band.

Figure 12 shows the block diagram of the FFT-based MRSS technique proposed in [22]. The chip area and power consumption are increased with multiple antenna architectures [22]; therefore, a single antenna receiver is used in this technique. In this method, the whole bandwidth of interest is digitized and input to the FFT-based sensing block [22]. The energy of each FFT is compared to a threshold and sensing is accomplished [22]. The medium access control block reconfigures the FFT-based sensing block and sensing is repeated.
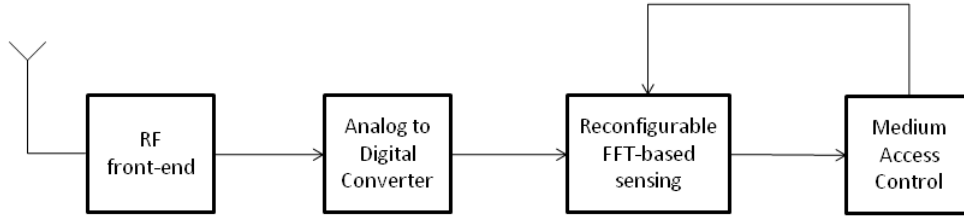
Figure 12.   Block Diagram of the FFT-based MRSS Method (From [22]).

The result of the multi-resolution spectrum sensing scheme applied individually by each node can be combined to achieve improved spectrum sensing. The next section explains the collaboration of the sensor nodes in spectrum sensing.

C.   COOPERATIVE SPECTRUM SENSING

Under fading or shadowing, received signal strength can be very low and this can prevent a node from sensing the signal of interest. Noise can also be a challenge when energy detection is used for spectrum sensing, although there are spectrum sensing techniques that are robust in the presence of noise, such as feature detection approaches [26]. Due to a low signal-to-noise ratio (SNR) value, the signal of interest may not be detected.

The idea of cooperative spectrum sensing in a RF sensor network is the collaboration of nodes on deciding the spectrum band used by the transmitters emitting the signal of interest. Nodes send either their test statistics or local decisions about the presence of the signal of interest to a decision maker, which can be another node. Through this cooperation, the unwanted effects of fading, shadowing and noise can be minimized [26]. This is because a signal that is not detected by one node may be detected by another. Figure 13 illustrates the cooperation of nodes in the detection of a signal of interest under shadowing and fading conditions. As the number of collaborating nodes increases, the probability of missed detection for all nodes decreases [27].

22
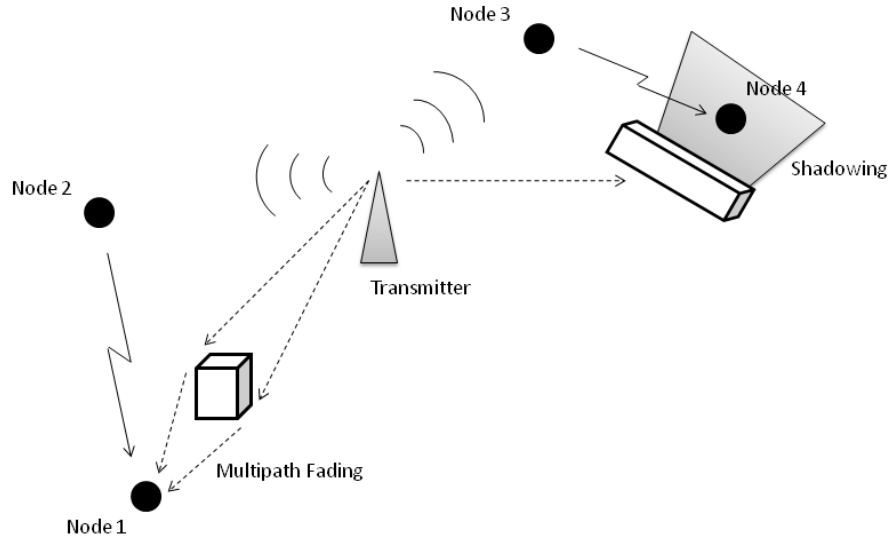
Figure 13.   Cooperation of Nodes to Detect the Signal of Interest under Fading and
Shadowing Conditions (After [8]).

Cooperation in spectrum sensing also improves the overall detection sensitivity of a RF sensor network without the requirement for individual nodes to have high detection sensitivity [26].   Less sensitive detectors on nodes means reduced hardware and complexity [26].

The trade-off for cooperation is more communication overhead [26]. Since the local sensing results of nodes should be collected at a decision maker, where the decision is made, a control channel is required between the decision maker and the other nodes [26].

There are two forms of cooperation in spectrum sensing: hard combination and soft combination. These two cooperation forms are also known as decision fusion and data fusion, respectively.   The difference between these two forms is the type of information sent to the decision maker.

The following subsections first introduce hard combination and soft combination schemes, which form the basis of the proposed three-bit hard combination scheme. Then, the three-bit hard combination scheme is explained in greater detail.

23

1. Hard Combination

In the hard combination scheme, local decisions of the nodes are sent to the decision maker. The algorithm for this scheme is as follows [27]. Every node first performs local spectrum sensing and makes a binary decision on whether a signal of interest is present or not by comparing the sensed energy with a threshold. All nodes send their one-bit decision result to the decision maker. Then, a final decision on the presence of the signal of interest is made by the decision maker.

Three of the rules used by the decision maker for a final decision are now discussed.

a. Logical-OR Rule

In this rule, if any one of the local decisions sent to the decision maker is a logical one (i.e., any one of the nodes decides that the signal of interest is present), the final decision made by the decision maker is one (i.e., decision maker decides that the signal of interest is present) [28].

b. Logical-AND Rule

In this rule, if all of the local decisions sent to the decision maker are one (i.e., all of the nodes decide that the signal of interest is present), the final decision made by the decision maker is one (i.e., decision maker decides that the signal of interest is present) [28].

c. Majority Rule

In this rule, if half or more of the local decisions sent to the decision maker are one (i.e., half or more of the nodes decide that the signal of interest is present), the final decision made by the decision maker is one (i.e., decision maker decides that the signal of interest is present) [28].

The performance analysis, in terms of the probability of detection and the probability of false alarm, for these decision rules can be found in the literature [28] and is not discussed here.

The major advantage of the hard combination scheme is that it requires only one bit of overhead [6]. Additionally, it only requires a low-bandwidth channel by which the decisions are sent [27]. But, since this low-bandwidth channel is also affected by fading and shadowing, a local sensing decision of binary one, showing the presence of a signal of interest, may be received as a binary zero, showing the absence of the signal [27]. This behavior degrades the detection performance [6].

2. Soft Combination

In the soft combination scheme, nodes send their sensing information directly to the decision maker without making any decisions [6]. The decision is made at the decision maker by the use of this information [6]. Soft combination provides better performance than hard combination, but it requires a wider bandwidth for the control channel [29]. It also requires more overhead than the hard combination scheme [6].

Two implementations of cooperative spectrum sensing schemes that use soft combination are given in [6] and [30]. In these schemes, the binary hypothesis test statistics of the nodes are sent to the decision maker and a global decision criterion is formed at the decision maker with the help of these local test statistics. The following development is a summary of the soft combination scheme proposed in [6].

In this scheme, the ith sample of the received signal of interest at the jth node is given by [6]

$$s_{ji} = \begin{cases} n_{ji}, & H_0 \\ \sqrt{P_{av,j}}\, a_{ji} + n_{ji}, & H_1 \end{cases}$$

where $1 \leq j \leq M$, M is the number of nodes, $1 \leq i \leq R$, R is the number of samples, $\sqrt{P_{av,j}}\, a_{ji}$ is the received signal of interest, $P_{av,j}$ is the average power of this received signal, a_{ji} is a Gaussian random variable with zero mean and unit variance, n_{ji} is white

25

noise, H_0 is the "Signal of interest does not exist" hypothesis, and H_1 is the "Signal of interest exists" hypothesis. After some assumptions, a test statistic, which is the observed energy at the jth node, is obtained as [6]

$$Y_j = \sum_{i=1}^{R} s_{ji}^2 = \begin{cases} b_{j0}, & H_0 \\ (1+P_{av,j})b_{j1}, & H_1 \end{cases} \qquad (1)$$

where b_{j0} and b_{j1} are central chi-square distributed random variables with R degrees of freedom. All nodes send their test statistics, given by Equation 1, to the decision maker. By applying Neyman-Pearson criterion, the global decision criterion is given by [6]

$$LR(Y) = \frac{\Pr(Y|H_1)}{\Pr(Y|H_0)} \underset{<}{\overset{>}{\underset{H_0}{\overset{H_1}{}}}} \eta$$

where $Y = (Y_1, Y_2, ..., Y_M)$ and η is the threshold calculated from the given probability of false alarm.

Combination schemes are still an active research area. Two-bit hard combination was recently proposed [6] and can be thought of as a hybrid combination scheme. The following subsection explains this scheme.

a.   Two-bit Hard Combination Scheme

The two-bit hard combination scheme [6] has the advantage of lower overhead, as demonstrated in hard combination approaches and greater performance gain, as demonstrated in soft combination approaches. It is also called softened two-bit hard combination [6]. The use of only one threshold in a hard combination scheme causes all nodes above the threshold to have the same weight regardless of observed energy differences between them [6]. The main idea behind the two-bit hard combination scheme is to divide the whole range of observed energy into more than two regions and to assign different weights to these regions [6]. By doing this, nodes that observe higher energies in upper regions have greater weights than nodes that observe lower energies in

26

lower regions [6].   Thus, the two-bit hard combination scheme outperforms the conventional one-bit hard combination scheme [6]. Also, this scheme has less communication overhead when compared to the traditional soft combination schemes in which test statistics are sent to the decision maker [6].

Figure 14 shows the thresholds and weights for different regions of a two bit hard combination scheme. There are three thresholds, as shown in Figure 14, which divide the range of observed energies into four regions [6]. For each region, the weights are defined as

$$w_0 = 0, \; w_1 = 1, \; w_2 = L, \; w_3 = L^2$$

where L is a design parameter [6]. The decision criterion, which is used to declare the presence of the signal of interest, is given by [6]

$$\sum_{h=0}^{3} w_h N_h \geq L^2$$

where N_h is the number of observed energies falling in region h. According to this decision criterion, if there is one observed energy in Region 3, while there are no observed energies in other regions, or L observed energies in Region 2, while there are no observed energies in other regions, or L^2 observed energies in Region 1, while there are no observed energies in other regions, the presence of the signal of interest is declared [6].
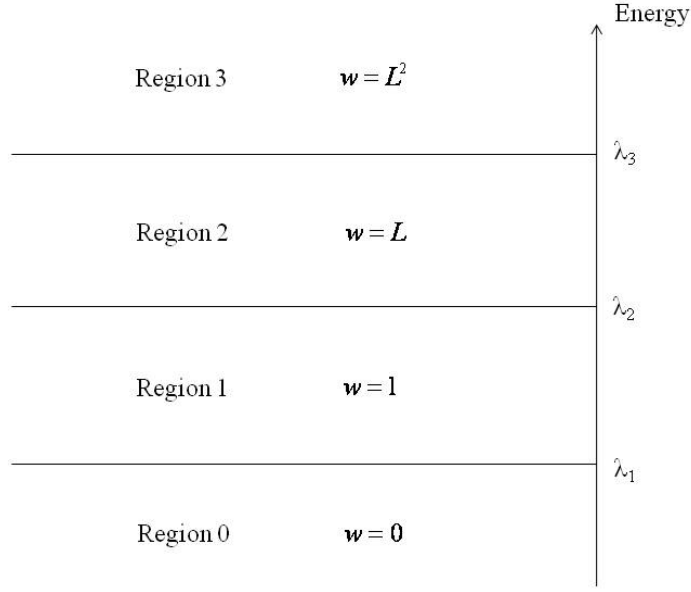
Figure 14.   Energy Regions of the Two-Bit Hard Combination Scheme (From [6]).

In this method, each node sends a two-bit information to the decision maker to inform it as to which region the observed energy fell [6]. The three thresholds are determined by using Neyman-Pearson criterion (to meet the target overall false alarm probability of all nodes in the network) and optimizing the detection performance [6]. A detailed threshold determination method is presented in [6].

b.   *Proposed Three-bit Hard Combination Scheme*

In this thesis, a new three-bit hard combination scheme for collaborative spectrum sensing is proposed. Using the main idea of the two-bit hard combination scheme proposed in [6], in this case the whole range of observed energy is divided into more than four regions. In particular, seven thresholds are used to divide the whole range of observed energy into eight regions. Each node sends to the decision maker a three-bit information that indicates the region in which its observed energy fell. Dividing the range of observed energy into more than eight regions causes each node to send more than three bits of information about the observed energy region, which means more overhead.

28

Figure 15 shows the eight regions and the corresponding three-bit representations. If a node observes an energy level falling in Region 7, it sends "111" to the decision maker. If a node observes an energy level falling in Region 0 it does not send any information to the decision maker.

Energy

Region 7	(111)	
		λ_7
Region 6	(110)	
		λ_6
Region 5	(101)	
		λ_5
Region 4	(100)	
		λ_4
Region 3	(011)	
		λ_3
Region 2	(010)	
		λ_2
Region 1	(001)	
		λ_1
Region 0		
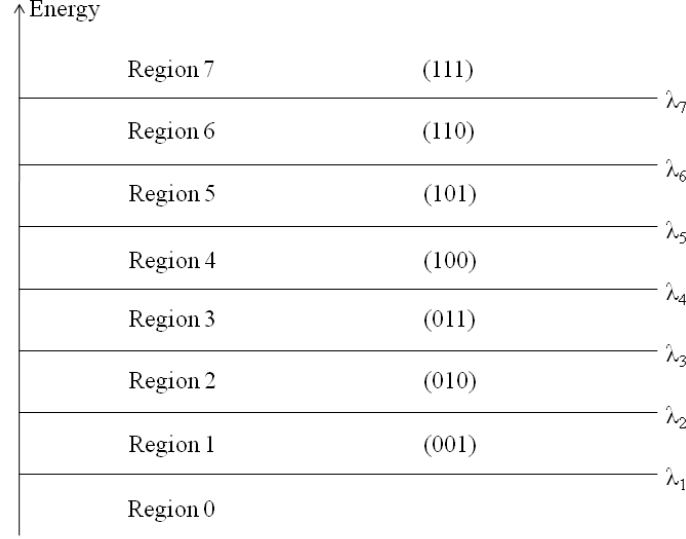
Figure 15.   Energy Regions of the Proposed Three-Bit Hard Combination Scheme.

Thresholds of the three-bit hard combination scheme are determined using the Neyman-Pearson criterion. Neyman-Pearson criterion is useful when the a priori probabilities and the cost assignments for each possible decision are difficult to assign [31]. In this criterion, while determining the threshold probability of false alarm p_{FA} is fixed to some value and the probability of detection p_D is maximized [31]. Table 1 shows the p_{FA} values chosen for determining the seven thresholds.

Threshold	False Alarm Value
λ_7	$\beta_7 p_{FA}$
λ_6	$\beta_6 p_{FA}$
λ_5	$\beta_5 p_{FA}$
λ_4	$\beta_4 p_{FA}$
λ_3	$\beta_3 p_{FA}$
λ_2	$\beta_2 p_{FA}$
λ_1	p_{FA}

Table 1.   Thresholds and the Corresponding False Alarm Values in the Three-Bit Hard Combination Scheme

The coefficients β_n in Table 1 are found by

$$\beta_n = (n-1)\times 10^{-(n-1)}, \qquad n = 2,...,7$$

where n is the threshold index and $\beta_1 = 1$.

The presence of the signal of interest is decided at the decision maker by use of the following equation

$$\sum_{h=1}^{7} w_h N_h \geq M \qquad (2)$$

where M is the total number of nodes in the network, N_h is the number of observed energies falling in region h and w_h is the weight value of region h shown in Table 2. In particular, if the weighted sum in Equation 2 is greater than M, then the signal of interest is declared as present.

Region	Weight
7	$w_7 = M$
6	$w_6 = 20$
5	$w_5 = 5$
4	$w_4 = 2.500$
3	$w_3 = 1.667$
2	$w_2 = 1.250$
1	$w_1 = 1$
0	$w_0 = 0$

Table 2.   Energy Regions and Corresponding Weights in the Three-Bit Hard Combination Scheme, where M is the Number of Nodes in the Network

Weights shown in Table 2 are determined in the following manner. If any one of the nodes observe energy in Region 7, with no observed energies in other regions, or 5% of all nodes observe energy in Region 6, with no observed energies in other regions, or 20% of all nodes observe energy in Region 5, with no observed energies in other regions, or 40% of all nodes observe energy in Region 4, with no observed energies in other regions, or 60% of all nodes observe energy in Region 3, with no observed energies in other regions, or 80% of all nodes observe energy in Region 2, with no observed energies in other regions, or 100% of all nodes observe energy in Region 1, with no observed energies in other regions, the signal of interest is said to be present. Table 3 summarizes the percentage of nodes required in a given region to declare the presence of the signal of interest, with no observed energies in other regions. While other percentage values are possible, the chosen values in Table 3 provided satisfactory results.

Region	Required number of nodes to declare the presence of signal of interest in a given region with no observed energies in other regions
7	1 node
6	5% of all nodes
5	20% of all nodes
4	40% of all nodes
3	60% of all nodes
2	80% of all nodes
1	100% of all nodes
0	-

Table 3.   Summary of the Weight Determination Approach used in this Thesis

Determining weights and thresholds are design issues. For example, Table 4 shows a different set of weights obtained by choosing a set of alternate percentage values. Likewise, a different set of coefficients in Table 1 can be used. For example,

$$\beta_n = 10^{-n}, \qquad n = 2,...,7$$

where n is the threshold index and $\beta_1 = 1$.

Region	Required number of nodes to declare the presence of signal of interest in a given region with no observed energies in other regions	Weight
7	1% of all nodes	$w_7 = 100$
6	5% of all nodes	$w_6 = 20$
5	10% of all nodes	$w_5 = 10$
4	20% of all nodes	$w_4 = 5$
3	30% of all nodes	$w_3 = 3.333$
2	40% of all nodes	$w_2 = 2.500$
1	50% of all nodes	$w_1 = 2$
0	-	$w_0 = 0$

Table 4.   An Alternate Design for Determining the Weights of the Three-Bit Hard Combination Scheme

D.   RECEIVED SIGNAL STRENGTH (RSS) - BASED LOCALIZATION

As mentioned in Chapter II.B, some of the RSS-based localization techniques require knowledge of the EIRP of the transmitter emitting the signal of interest. This can be a limitation in using this technique for systems in which the EIRP of the signal of interest source is unknown, such as the scenario shown in Figure 1. This section explains the RSS-based localization approach [5] used in the proposed sensor network based cooperative wideband spectrum sensing and localization scheme. This localization approach does not require the EIRP of the transmitter emitting the signal of interest [5].

Figure 16 shows the network configuration proposed in [5]. In this network configuration, it is implicitly assumed that the radiation patterns of the transmitter antennas are azimuthally omni-directional. In this scheme at least four nodes, whose positions are known, must measure the RSS values from the signal of interest source [5]. Since every node sends its RSS measurement value and its position information to all other nodes, localization procedures can be applied on any node [5].
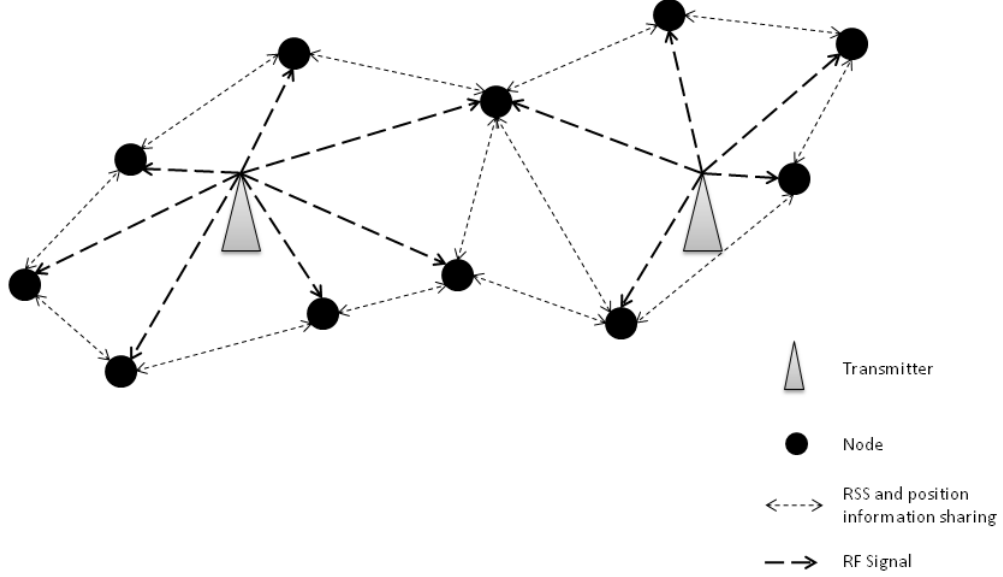
Figure 16.   A Planar Network Configuration for RSS-based Localization (From [5]).

The ideal RSS value at the jth node is equal to the ideal received power, $P_{r,j}^{ideal}$, which is given by [5]

$$P_{r,j}^{ideal} = C_j \frac{P_t}{d_j^\alpha}, \qquad j = 1,2,...M \qquad (3)$$

where P_t is the EIRP of the transmitter, C_j is a constant representing the factors effecting RSS, such as antenna gain and height, α is the path loss exponent, and d_j is the distance between the transmitter and the jth node, represented by $d_j = \sqrt{(x-x_j)^2 + (y-y_j)^2}$ where (x,y) is the real position of the transmitter and (x_j, y_j) is the position of the jth node.

The following process is applied to find the position of the transmitter. First $d_j = \sqrt{(x-x_j)^2 + (y-y_j)^2}$ is substituted into Equation 3 [5], yielding

$$\frac{C_j}{P_{r,j}^{ideal}} = \frac{[(x-x_j)^2 + (y-y_j)^2]^{\alpha/2}}{P_t} \quad , \qquad j = 1, 2 \ldots M$$

Taking the $2/\alpha$ power of both sides [5] yields

$$\left(\frac{C_j}{P_{r,j}^{ideal}}\right)^{2/\alpha} = \frac{(x-x_j)^2 + (y-y_j)^2}{(P_t)^{2/\alpha}}, \qquad j = 1, 2 \ldots M$$

$$= \frac{x^2 + y^2 - 2xx_j - 2yy_j + x_j^2 + y_j^2}{(P_t)^{2/\alpha}}$$

Isolating the $x_j^2 + y_j^2$ term results in [5]

$$x_j^2 + y_j^2 = 2xx_j + 2yy_j + \left(\frac{C_j}{P_{r,j}^{ideal}}\right)^{2/\alpha} (P_t)^{2/\alpha} - \left(x^2 + y^2\right), \qquad j = 1, 2, \ldots M$$

Since this last equation holds at each node, it can be extended to all nodes and expressed in matrix form as [5]

$$
\begin{bmatrix}
2x_1 & 2y_1 & \dfrac{C_1}{P_{r,1}^{ideal}}^{2/\alpha} & -1 \\
2x_2 & 2y_2 & \dfrac{C_2}{P_{r,2}^{ideal}}^{2/\alpha} & -1 \\
\vdots & \vdots & \vdots & \vdots \\
2x_M & 2y_M & \dfrac{C_M}{P_{r,M}^{ideal}}^{2/\alpha} & -1
\end{bmatrix}
\begin{bmatrix}
x \\ y \\ (P_t)^{2/\alpha} \\ x^2 + y^2
\end{bmatrix}
=
\begin{bmatrix}
x_1^2 + y_1^2 \\ x_2^2 + y_2^2 \\ \vdots \\ x_M^2 + y_M^2
\end{bmatrix}
\qquad (4)
$$

This linear equation can be solved by using the least squares method [5]. The solution of Equation 4 not only provides the position of the transmitter but also its EIRP. In particular, the $(P_t)^{2/\alpha}$ value is found. Once solved, the obtained x, y, and P_t quantities are termed as x_{est}, y_{est}, and P_{est}, respectively.

34

The shadowing effect is included using the log-normal path loss model, which is given by [5]

$$P_{r,j} = C_j \frac{P_t}{d_j^\alpha S_j}, \qquad\qquad j = 1, 2, ... M$$

where $S_j = 10^{0.1X_j}$ is a log-normal random variable, X_j is a Gaussian random variable, whose mean is zero and variance σ^2, and the other parameters are the same as in Equation 3. To minimize the unwanted effect of shadowing, RSS values ($P_{r,j}$ values) are averaged as given by [5]

$$P_{r,j}^{ideal} \approx \frac{1}{R} \sum_{i=1}^{R} P_{r,ji} \qquad\qquad (5)$$

where R is the total number of samples and $P_{r,ji}$ is the ith sample RSS value at the jth node in dBm.

E.   SUMMARY

This chapter presented the proposed sensor network based cooperative wideband spectrum sensing and localization scheme. It was followed by a discussion of the fundamental techniques and approaches used in this scheme. In particular, the MRSS, cooperative spectrum sensing, proposed three-bit hard combination and RSS-based localization schemes were discussed.

The simulation model and simulation results are presented in the next chapter. The objective of the next chapter is to implement the proposed sensor network based cooperative spectrum sensing and localization scheme and analyze its performance.

THIS PAGE INTENTIONALLY LEFT BLANK

IV. SIMULATION MODEL AND RESULTS

In Chapter III, the proposed sensor network based cooperative wideband spectrum sensing and localization scheme, which uses wavelet-based multi-resolution spectrum sensing (MRSS) [4], three-bit hard combination, and received signal strength (RSS)-based localization [5] was presented. This chapter presents the simulation scenario, followed by the simulation model developed to implement the proposed scheme. Next, simulation results are presented. In particular, the effects of window type, number of power spectral densities (PSDs) averaged, number of nodes, signal-to-noise ratio (SNR), and number of transmitters on detection performance of the cooperative wideband spectrum sensing part of the proposed scheme are discussed. The effects of the number of samples, number of nodes, and standard deviation of the Gaussian random variable in shadowing model σ, on performance of the localization part of the proposed scheme are also discussed.

A. SIMULATION SCENARIO

This section describes the simulation scenario presented in Figure 1. The scenario is shown in greater detail in Figure 17. In this scenario, the RF sensor nodes are deployed randomly over an area of interest and they detect signals of interest in the air and determine the spectral bands of these signals. Additionally, the positions and effective isotropic radiated powers (EIRPs) of the transmitters emitting these signals are estimated. To accomplish its tasks, the sensor network applies the proposed sensor network based cooperative wideband spectrum sensing and localization scheme presented in Chapter III.A. Figure 17 presents a typical scenario for military applications, since the RF sensor network is deployed away from the transmitters.

The following assumptions apply to this simulation scenario:

1. After the sensor nodes are deployed, the positions of the nodes are calculated and a node is designated as decision maker.

2. Before the localization process starts, RSS values at each node due to the transmitters are measured.

3. The distances between the nodes are more than the half of the wavelength of the signal of interest.
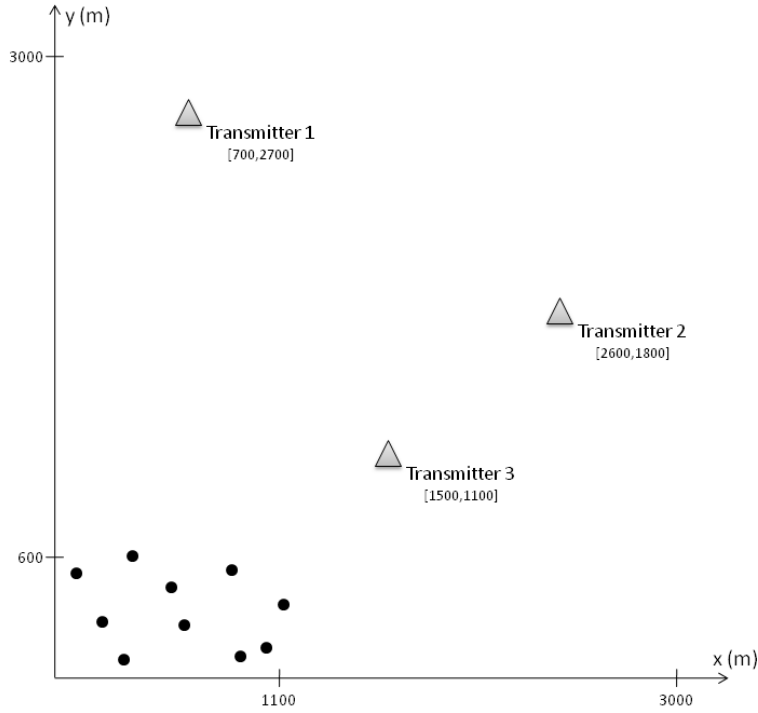
Figure 17.   Simulation Scenario.

The algorithm of the proposed scheme presented in Chapter III.A is summarized here for convenience. Firstly, the decision maker node determines seven thresholds. Secondly, all nodes, except for the decision maker, apply coarse resolution spectrum sensing to the entire bandwidth of interest. Then, each of these nodes determines the three-bit local observation values by applying the seven thresholds and sends them to the decision maker. The decision maker determines the occupied spectrum bands and selected nodes then apply fine resolution spectrum sensing on these spectrum bands. Through fine resolution sensing, the frequency bands of the signals in the air are

38

determined. To find the positions of the transmitters emitting these signals, the decision maker applies the RSS-based localization scheme by using the averaged RSS values and node positions.

B.   SIMULATION MODEL

Figure 18 and Figure 19 depict the simulation block diagrams of the cooperative wideband spectrum sensing part and the localization part of the proposed sensor network based cooperative wideband spectrum sensing and localization scheme, respectively.

The implementation of the "determination of seven thresholds," "coarse resolution sensing," and "fine resolution sensing" blocks in Figure 18 is carried out by using the wavelet-based MRSS scheme [4] discussed in Chapter III.B.1. Threshold determination takes place at the decision maker. Coarse resolution sensing is applied by all nodes except the decision maker, whereas only selected nodes apply fine resolution sensing. The implementation of the "determination of the three-bit values" and "three-bit hard combination" blocks in Figure 18 is carried out by using the proposed three-bit hard combination scheme discussed in Chapter III.C.3. Three-bit values are determined by the nodes after the coarse resolution sensing. Three-bit hard combination takes place at the decision maker. The "fine resolution sensing" block is applied to determine the frequency band of the signal. The "RSS measurement" and "calculation of node positions" blocks in Figure 19 are not implemented in this thesis; therefore the RSS measurements and node positions are assumed to be given. The function of the "averaging" block is to minimize the unwanted effect of shadowing. The implementation of the "RSS-based localization" block is carried out by using the scheme [5] explained in Chapter III.D. The model was implemented in MATLAB programming language. The following subsections describe each of the blocks shown in Figure 18 and Figure 19.
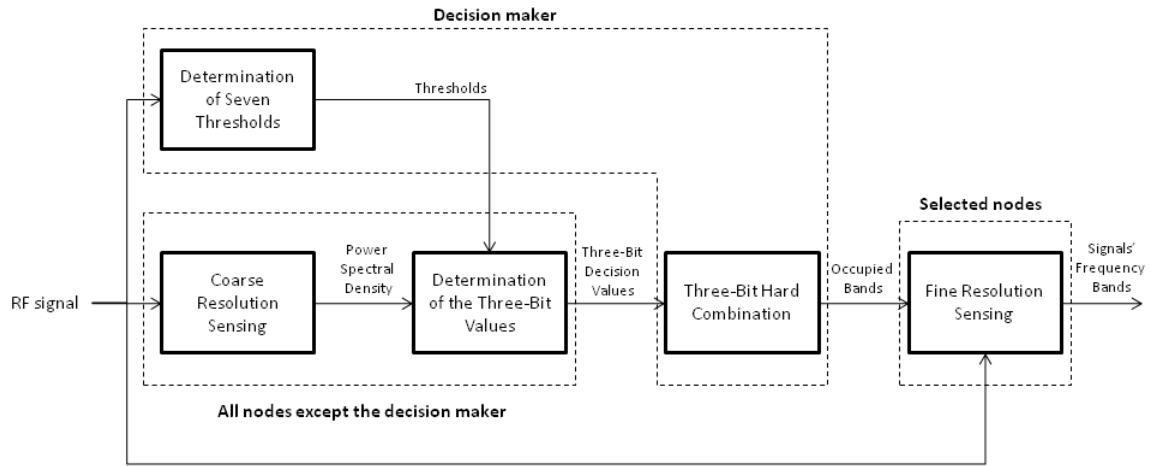
Figure 18.   Simulation Block Diagram of the Cooperative Wideband Spectrum Sensing Part of the Proposed Scheme.
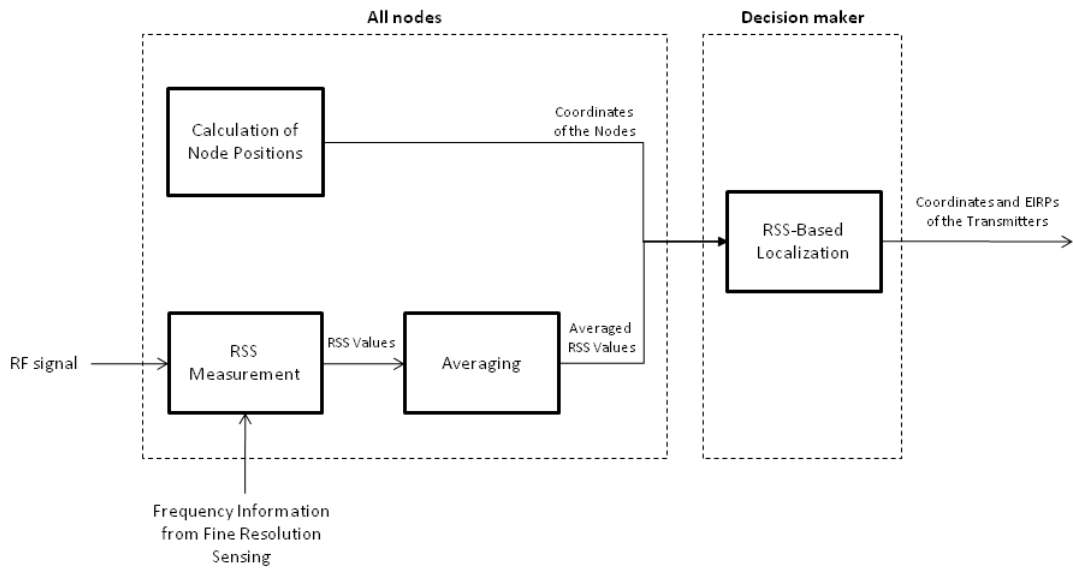
Figure 19.   Simulation Block Diagram of the Localization Part of the Proposed Scheme.

40

1.   Cooperative Wideband Spectrum Sensing

a.   Determination of Seven Thresholds

Figure 20 shows the multi-resolution spectrum sensing [4] diagram for the implementation of the "determination of seven thresholds" block of Figure 18. This block diagram consists of a low noise amplifier (LNA), a window (wavelet) generator, a cosine function generator, multipliers, integrators and an envelope detector. In determining seven thresholds, a noise only input is considered.
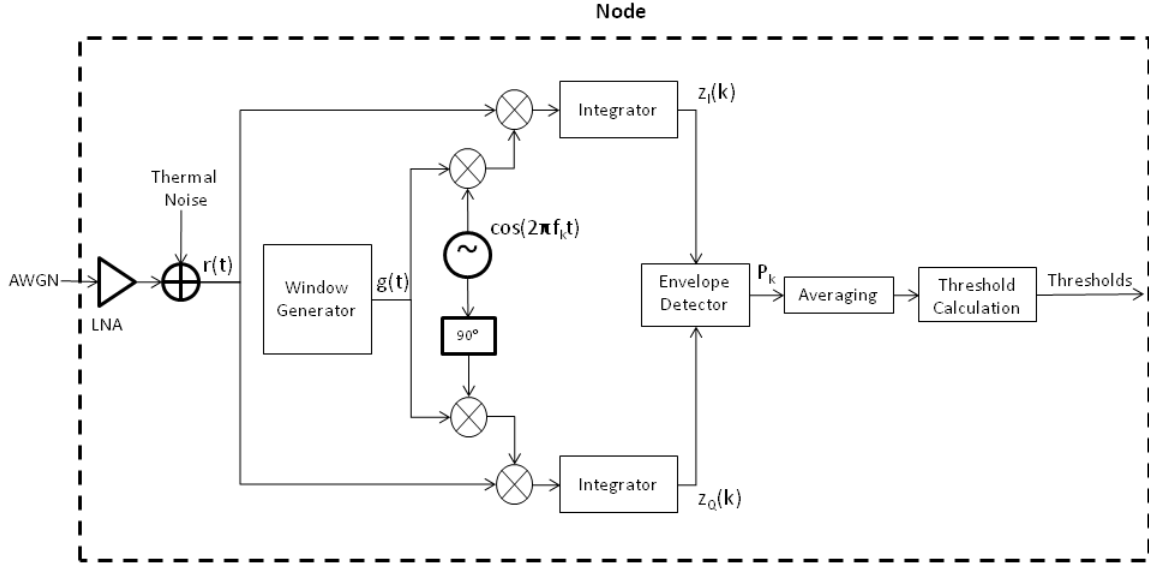
Figure 20.   Multi-Resolution Spectrum Sensing Diagram for the Implementation of "Determination of Seven Thresholds" Block (After [24]).

For the LNA, gain and noise figure values are assumed to be $G_{dB} = 40$ and $F_{dB} = 5$, respectively. Thermal noise is given by [32]

$$N_{Thermal} = G \kappa T_{Sys}^{\circ} B$$

where G is the gain of the LNA, $\kappa = 1.38 \times 10^{-23}$ J/K is the Boltzmann constant, T_{Sys}° is the system temperature, and B is the bandwidth of the system. System temperature is given by [32]

$$T_{Sys}^{\circ} = T_{Ant}^{\circ} + T_{Line}^{\circ} + L_F T_{PreAmp}^{\circ} \tag{6}$$

where T_{Ant}° is the antenna temperature, T_{Line}° is the line temperature, L_F is the line-loss factor, and T_{PreAmp}° is the preamplifier temperature. Assuming a lossless line between the antenna and the LNA, and that the antenna temperature is 290K°, Equation 6 becomes

$$T_{Sys}^{\circ} = 290\text{K}^{\circ} + T_{PreAmp}^{\circ}$$

where $T_{PreAmp}^{\circ} = (F-1) \times 290\text{K}^{\circ}$. After substituting $F = 3.16$ into this equation, the system temperature is calculated as $T_{Sys}^{\circ} = 916.4\text{K}^{\circ}$. The thermal noise value follows as

$$N_{Thermal\_dB} = G_{dB} + \kappa_{dB} + T_{Sys\_dB}^{\circ} + B_{dB} \tag{7}$$

where $G_{dB} = 40$, $\kappa_{dB} = -228.60$ and $T_{Sys\_dB}^{\circ} = 29.62$. Since the window length in threshold determination is 0.1 µs, which corresponds to a 10 MHz system bandwidth, the thermal noise value is determined as -88.98 dB.

As will be explained in Chapter IV.C.1, a rectangular window is used since it is found to provide a high detection margin. The rectangular window is defined by [33]

$$W[n] = \begin{cases} 1, & 0 \le n \le N_w \\ 0, & \text{otherwise} \end{cases}$$

where the window length is equal to $N_w + 1$. Window pulse length T_g is equal to $(N_w + 1)/f_s$, where f_s is the sampling frequency. Note that T_g is changed to apply multi-resolution spectrum sensing. Sampling frequency f_s is chosen as 1 GHz. The frequency spectrum of interest is assumed to be between $f_{start} = 31$ MHz and $f_{stop} = 130$ MHz.

Outputs of the integrators are given by

42

$$z_I(k) = \frac{1}{T_g} \int_0^{T_g} \left[r(t)\{g(t)\cos(2\pi f_k t)\} \right] dt \qquad \text{for } k = 0,...,K$$

$$z_Q(k) = \frac{1}{T_g} \int_0^{T_g} \left[r(t)\{g(t)\sin(2\pi f_k t)\} \right] dt \qquad \text{for } k = 0,...,K$$

where $g(t)$ is the rectangular window pulse with length T_g, $f_k = (31 \times 10^6 + kf_{sweep})$ and $K = \text{Round}[(130\,\text{MHz} - 31\,\text{MHz})/f_{sweep}]$. For determination of seven thresholds, f_{sweep} and T_g values are chosen as 5 MHz and 0.1 μs, respectively.

The envelope detector in Figure 20 outputs a Rayleigh distributed variable when the input is a Gaussian random variable [34]. The output of the envelope detector is given by

$$P_k = \sqrt{z_I^2(k) + z_Q^2(k)} \,.$$

To improve the performance of the MRSS scheme, P_k, which provides an estimate of PSD, is calculated by averaging over Q values [4].

While determining thresholds, the distributions of the "noise only" inputs at the envelope detector are assumed Gaussian with zero mean and a variance of σ^2. With this assumption, the output of the envelope detector has a Rayleigh distribution with scale parameter σ. A Rayleigh distribution with scale parameter σ is identical to a Weibull distribution with shape parameter 2 and scale parameter $\sqrt{2}\sigma$ [35]. Thresholds are the values limiting the areas under the probability density function of this output distribution. In particular, the thresholds are determined by calculating the areas under the Weibull distribution for different p_{FA} values given in Table 1. Then these threshold values are converted to dB values by taking the logarithm and multiplying by 10. An alternate method to determine the thresholds is by finding the areas under the extreme value distribution, which is also known as a log-Weibull distribution, and then multiplying them by 10.

43

b. *Coarse Resolution Sensing*

After the thresholds are determined and the nodes are informed about these threshold values, the "coarse resolution sensing" block is implemented by using the diagram shown in Figure 21 to quickly examine the spectrum. Parameters f_{sweep} and T_g are chosen as 2 MHz and 2 μs, respectively. Power spectral density (PSD) is obtained from the output of Figure 21.

In Figure 21, to generate the RF signal, for simplicity, each transmitter is assumed to broadcast the same information signal. The length of the RF signal is assumed to be equal to the window length. The ideal received power (i.e., ideal RSS value) at each node is given by Equation 3. In Equation 3, P_t values for each transmitter are assumed to be 1 W, and C_j constants for all nodes and the path loss exponent α are chosen as 1 and 3, respectively. Table 5 lists the transmitter specifications; note that the signals generated by each transmitter use different modulation schemes. Distance values in Equation 3 are calculated using the positions of the transmitters and nodes as given in Table 6. Sampling frequency is assumed to be 1 GHz.

The shadowing effect is included using the log-normal path loss model given by [5]

$$P_{r,j} = \frac{P_{r,j}^{ideal}}{S_j} \qquad (8)$$

where $P_{r,j}$ is the received power (RSS value) at the jth node, $S_j = 10^{0.1 X_j}$ is a log-normal random variable, and X_j is a Gaussian random variable whose mean is zero and variance is σ^2. The thermal noise value for coarse resolution sensing is calculated as -101.99 dB from Equation 7 by setting the system bandwidth to 0.5 MHz.
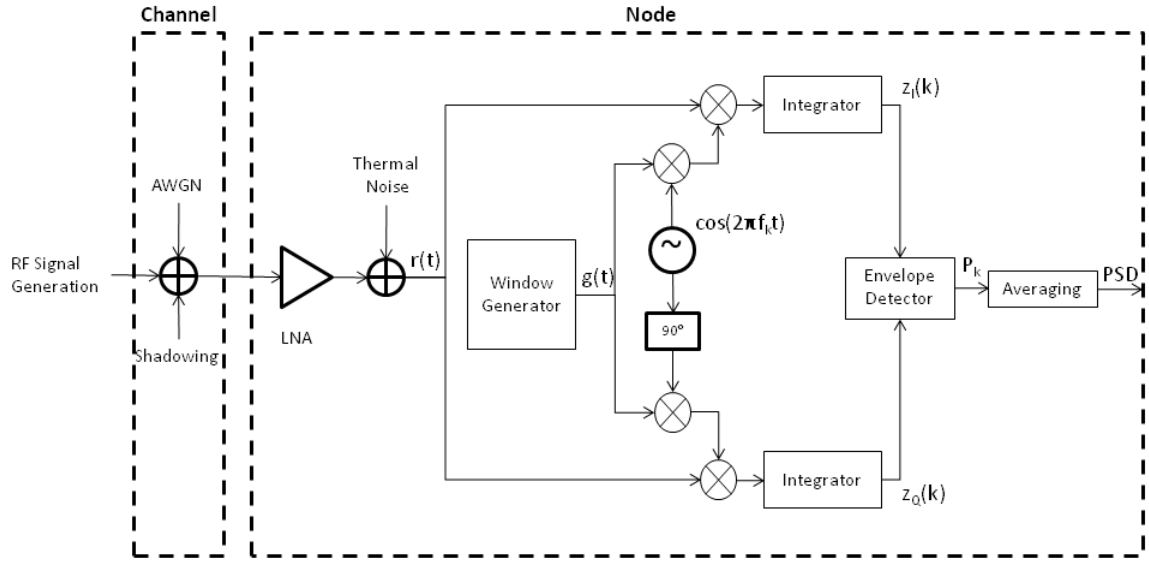
Figure 21.   Multi-Resolution Spectrum Sensing Diagram for the Implementation of "Coarse Resolution Sensing" Block (After [24]).

Transmitter	Modulation	EIRP (W)	Frequency (MHz)	x coordinates (m)	y coordinates (m)
Transmitter 1	PM	1	41	700	2700
Transmitter 2	64QAM	1	105	2600	1800
Transmitter 3	16QAM	1	95	1500	1100

Table 5.   Transmitter Specifications

Node	x coordinates (m)	y coordinates (m)
1	700	250
2	900	100
3	1000	200
4	300	100
5	200	300
6	1100	400
7	500	450
8	800	500
9	100	550
10	400	600
11	100	50
12	800	150
13	500	200
14	200	200
15	50	300
16	600	350
17	900	400
18	150	450
19	700	500
20	1000	600

Table 6.   Coordinates of the Nodes

c.   *Determination of Three-bit Values*

After the coarse resolution sensing, the "determination of three-bit values" block follows. The result of the coarse resolution sensing is compared with the seven thresholds and three-bit values are determined for each frequency value at every node. Figure 15 shows the energy regions with the corresponding three-bit local observation values that will be sent to the decision maker when there is an observed energy in that region.

d.   *Three-bit Hard Combination*

The function of the "three-bit hard combination" block in Figure 18 is to combine the sensing results of the nodes and to detect the signals in the air by using the

proposed three-bit hard combination scheme at the decision maker. The decision criterion given by Equation 2 and the weights given in Table 2 are used to determine the presence of the signal of interest.

e.   *Fine Resolution Sensing*

As a last stage, the "fine resolution sensing" block is implemented with the same diagram used for the "coarse resolution sensing" block shown in Figure 21. The objective of fine resolution sensing is to determine the frequency band of the signal. The differences from coarse resolution sensing are the values of f_{sweep} and T_g, which are chosen as 500 kHz and 4 μs, respectively. The result of the three-bit hard combination scheme determines the spectrum bands on which fine resolution sensing will be applied, and the nodes that will apply fine resolution sensing. Then, fine resolution sensing is applied on these spectrum bands by the nodes that sense the highest energies in these bands.

2.   RSS-Based Localization

Figure 19 shows the simulation block diagram for the localization part of the proposed scheme. As mentioned earlier, RSS measurement and calculation of node positions are not implemented in this thesis, but they are assumed to be given.

a.   *Averaging*

The function of the "averaging" block in Figure 19 is simply to minimize the shadowing effect. As in the cooperative wideband spectrum sensing part, shadowing effect is included by the log-normal path loss model given by Equation 8. RSS values are averaged using Equation 5.

b.   *RSS-Based Localization*

The "RSS-based localization" block in Figure 19 is implemented by solving Equation 4. As in Chapter IV.B.1.b, we assume that C_j values for all nodes are

equal to 1, path loss exponent α is 3, and node positions are as shown in Table 6. Note that RSS values at each node, $P_{r,j}$, are assumed to be given.

A least squares method [5] is used to solve Equation 4. If we define the components of Equation 4 as

$$
\Lambda = \begin{bmatrix}
2x_1 & 2y_1 & \dfrac{C_1}{P_{r,1}^{ideal}}^{2/\alpha} & -1 \\[2ex]
2x_2 & 2y_2 & \dfrac{C_2}{P_{r,2}^{ideal}}^{2/\alpha} & -1 \\[1ex]
\vdots & \vdots & \vdots & \vdots \\[1ex]
2x_M & 2y_M & \dfrac{C_M}{P_{r,M}^{ideal}}^{2/\alpha} & -1
\end{bmatrix}, \quad
\theta = \begin{bmatrix}
x \\
y \\
(P_t)^{2/\alpha} \\
x^2 + y^2
\end{bmatrix} \quad \text{and} \quad
\Phi = \begin{bmatrix}
x_1^2 + y_1^2 \\
x_2^2 + y_2^2 \\
\vdots \\
x_M^2 + y_M^2
\end{bmatrix}
$$

we obtain

$$
\Lambda \cdot \theta = \Phi \tag{9}
$$

Since matrix Λ in Equation 9 may not have full rank, implying that the least-squares solution may not be unique [35], implementation of least squares method is accomplished by a pseudo-inverse approach:

$$
\theta = \Lambda^{\dagger} \Phi
$$

where $\Lambda^{\dagger}$ is the Moore-Penrose pseudo-inverse matrix of Λ, which provides the minimal norm solution [35].

C.   COOPERATIVE WIDEBAND SPECTRUM SENSING RESULTS

Coarse resolution sensing, which is applied with the three-bit hard combination to detect signals in the air, and fine resolution sensing, which is used to determine the frequency bands of these signals, are the two most important functions of cooperative wideband spectrum sensing. This section starts with the results of coarse and fine resolution sensing applied at the sensor nodes. Then, the simulation results of the cooperative wideband spectrum sensing part of the proposed scheme are presented. In

particular, the effects of window type, number of PSDs averaged, number of nodes, SNR, and number of transmitters on detection performance of the cooperative wideband spectrum sensing part of the proposed scheme are evaluated.

The SNR definition given by

$$SNR = 10\log_{10}\left(\frac{\text{Signal Power}}{\text{Noise Power}}\right)$$

is used throughout this thesis.

Figure 22 shows the result of coarse resolution sensing, with the parameters given in Chapter IV.B.1.b, applied between a 31 MHz and 130 MHz band at Node 2. The three peak values at 41 MHz, 95 MHz, and 105 MHz correspond to the three transmitters whose specifications are given in Table 5. Figure 22 also shows the seven thresholds that divide the whole range of observed energy into eight regions defined in Figure 15. As can be seen from Figure 22, the observed energies at 41 MHz, 95 MHz and 105 MHz are in regions 0, 7 and 1, respectively. With this information, it can be deduced that Node 2 will send a three-bit local observation value of "111" for 95 MHz and "001" for 105 MHz. Since the observed energies at other frequencies are in Region 0, no information will be sent to the decision maker for these frequencies. Table 7 summarizes the local observation values formed at Node 2.

Frequency	Region of Observed Energy	Three-Bit Local Observation Value
41 MHz	0	-
95 MHz	7	111
105 MHz	1	001
Other	0	-

Table 7.   Summarization of Local Observation Values formed by Node 2
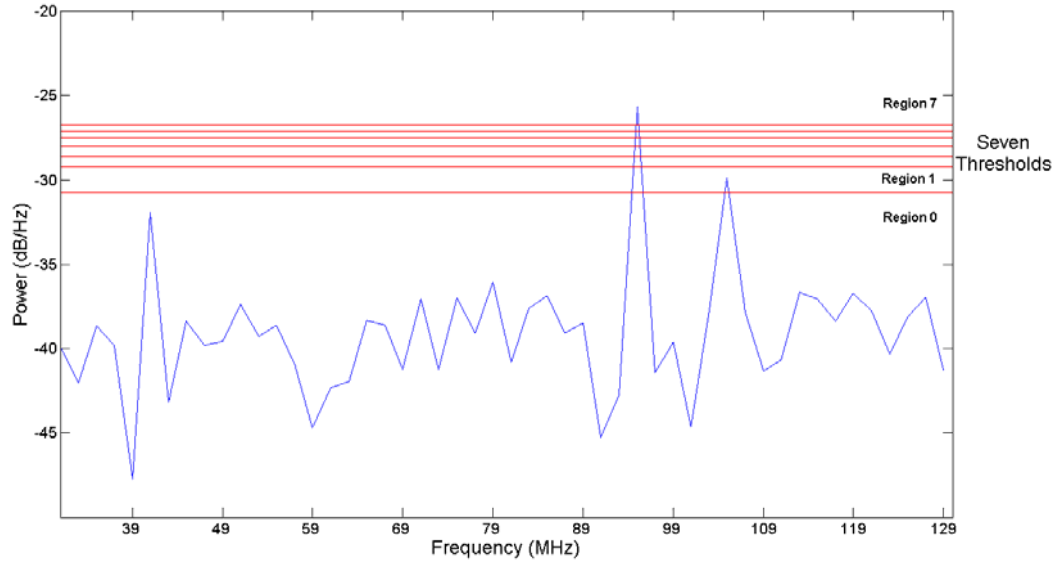
Figure 22.   Result of Coarse Resolution Sensing of a 31 – 130 MHz band at Node 2.

If we assume that after the coarse resolution sensing stage that the node sensing the highest energy between 91 MHz and 100 MHz band is Node 2, the decision maker will demand from Node 2 a fine resolution sensing of 91 to 100 MHz band. Figure 23 shows the result of fine resolution sensing applied by Node 2 on the 91 – 100 MHz band. The parameters used for this fine resolution sensing can be found in Chapter IV.B.1.e. The maximum threshold value below the maximum observed energy determined by coarse resolution sensing on 91 to 100 MHz band, which is Threshold 7, is also shown in Figure 23. The peak value in the plot shows that the frequency of the signal is 95 MHz and its bandwidth is less than 500 kHz, since the resolution of fine resolution sensing is chosen to be 0.5 MHz.
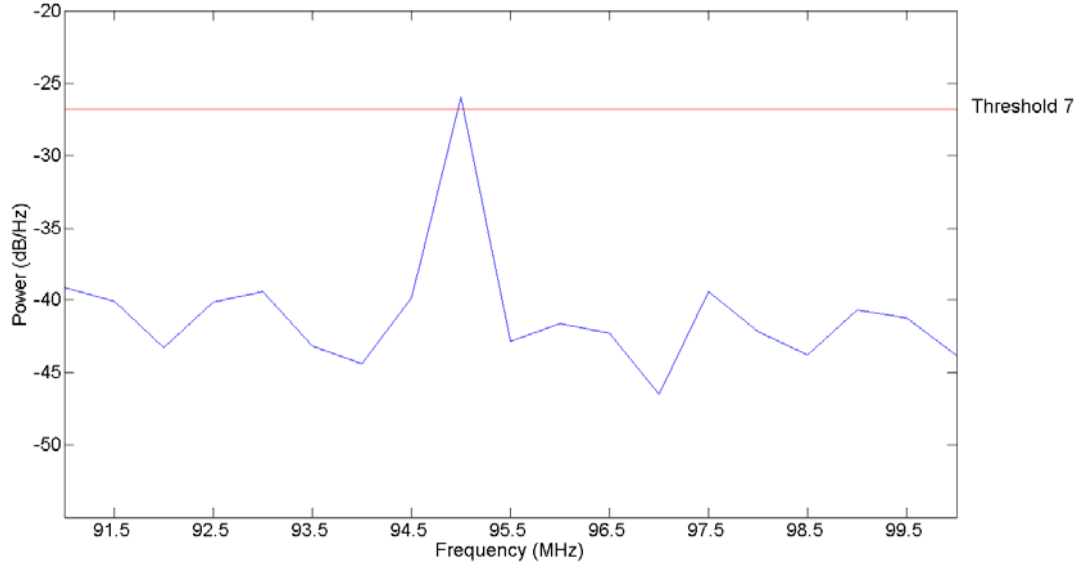
Figure 23.   Result of the Fine Resolution Sensing of 91 – 100 MHz at Node 2.

In the following subsections, except for the effect of window type, detection percentage is used as a detection performance measure, simulations are run 1000 times, the standard deviation σ of the Gaussian variable in Equation 8 is set to 10 and the probability of false alarm is chosen as 0.1. Detection percentage is defined as

$$D_{\%} = \frac{\text{Number of detections of Transmitter 3}}{\text{Number of Simulation Runs}} \times 100 \qquad (10)$$

While studying the effect of window type, detection margin is used as a performance measure, the simulation is run for 10,000 times, the standard deviation σ of the Gaussian variable in Equation 8 is set to 1 and the probability of false alarm is chosen as 0.1. Detection margin is defined as

$$D_M = \left(\begin{array}{c} \text{Observed energy at 95 MHz} \\ \text{with coarse resolution sensing} \end{array} \right) - \left(\text{7th threshold value} \right)$$

For all simulations, except in Chapter IV.C.5, for simplicity, only one transmitter, Transmitter 3, as specified in Table 5, is assumed to emit a signal. The values of the other parameters are the same as given in Chapter IV.B.1.b.

1. Effect of Window Type

In the implementation of the "determination of seven thresholds," "coarse resolution sensing," and "fine resolution sensing" blocks, a window is generated as shown in Figure 20 and Figure 21. The effect of the type of the window is studied by measuring the energy level at 95 MHz with coarse resolution spectrum sensing, and calculating the detection margin above the seventh threshold at Node 2, while the number of PSDs is 10 and the SNR is equal to 0.

Figure 24 shows the detection margin measurements for different windows. As can be seen from this figure, a rectangular window provides the best detection margin at a value of 7.268 dB above the seventh threshold. Using a Kaiser window, a very close detection margin of 7.258 dB is obtained. The Flattop window provides the least detection margin at a value of 4.477 dB. The results for the Blackman-Harris and Hamming windows fall in between these values. Based on these results, a rectangular window is used in all of the simulations in this thesis.
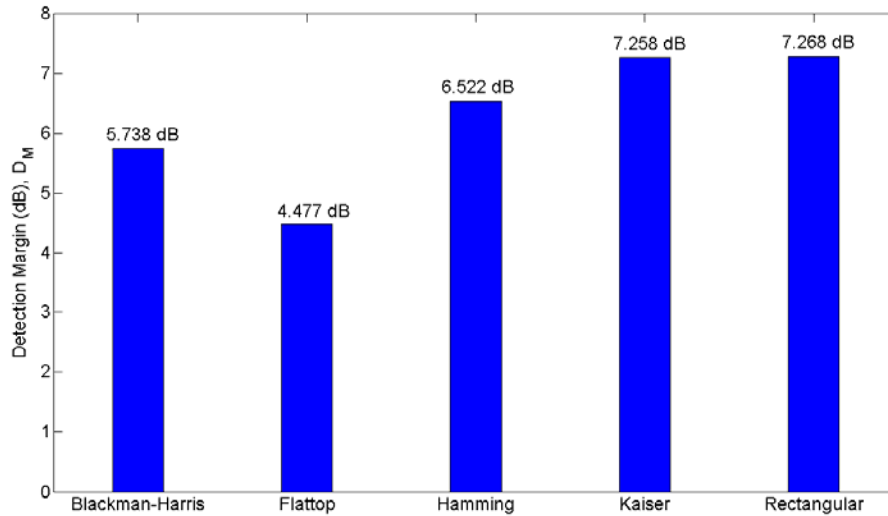
Figure 24.   Detection Margin versus Window Type.

52

2. Effects of Number of PSDs Averaged

In Chapter III.B.1, it is mentioned that by calculating P_k, which represents the PSD at frequency f_k, more than once and then averaging the results, a reduced noise floor level and more discernable signal spectra is obtained [4]. As mentioned in Chapter IV.B.1.a, P_k is calculated Q times and then averaged, so Q is the number of PSDs averaged.

Figure 25 depicts the effect of the number of PSDs averaged on detection percentage as a function of the number of nodes participating in cooperative wideband spectrum sensing at $SNR = -20\text{ dB}$. Figure 26 shows the plots of detection percentage versus number of PSDs averaged for different SNR values when there are ten nodes participating in the cooperative wideband spectrum sensing. Both figures indicate that when the number of PSDs averaged is increased, the detection percentage increases. This result is consistent with the expected effect of the averaging.

In Figure 25, when the number of PSDs averaged is less than twenty, eight nodes perform better detection than twelve or sixteen nodes. This is due to the positions of the nodes and the applied decision criterion, and will be explained in greater detail in Chapter IV.C.3.
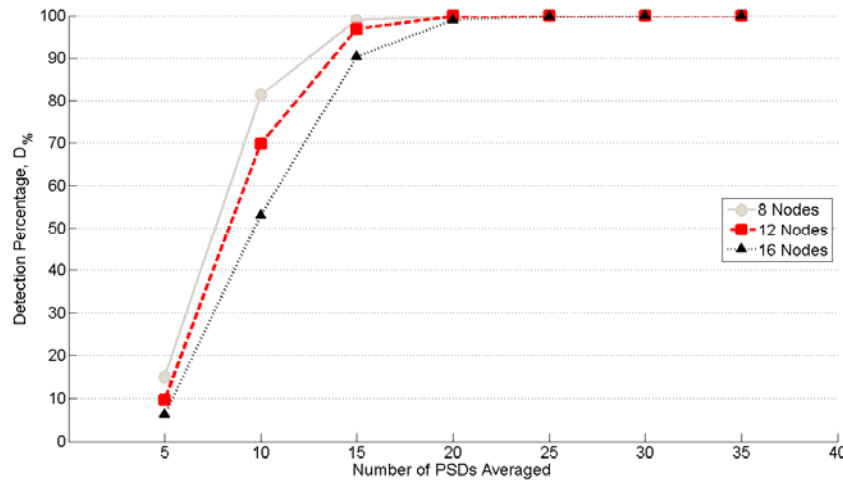
Figure 25.   Detection Percentage versus Number of PSDs Averaged for Three Different Number of Nodes.

Figure 26 shows that for a particular number of PSDs averaged, when the SNR is low, the detection percentage degrades; however, if the number of PSDs averaged is increased, detection performance can be improved. These are expected results for energy detectors and will be explained in further detail in Chapter IV.C.4.
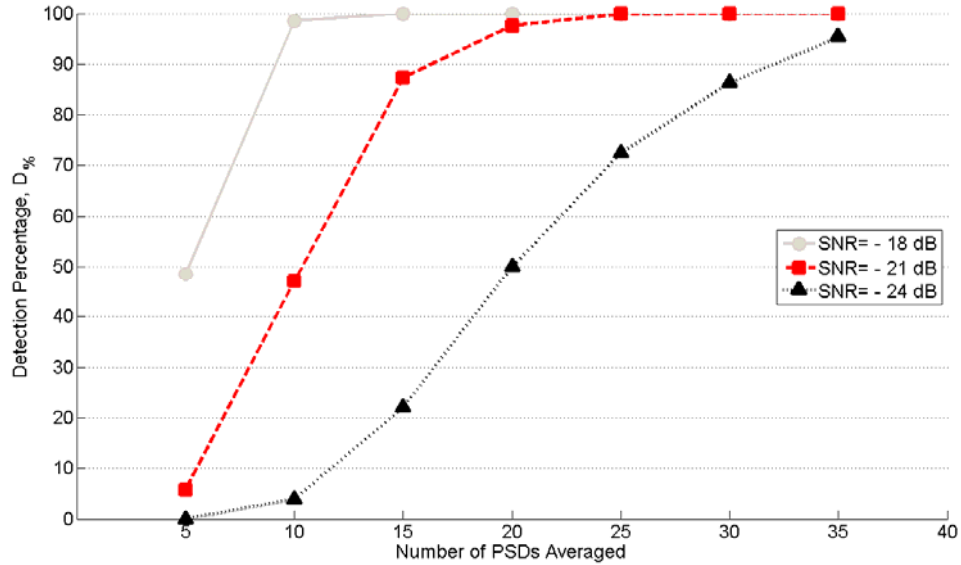
Figure 26.   Detection Percentage versus Number of PSDs Averaged for Three Different SNR Values.

3.   Effects of Number of Nodes

Because of scarce battery energy or environmental effects, sensor nodes fail in wireless sensor networks [36]. In these cases the number of nodes participating in the cooperative wideband spectrum sensing can change.

Figure 27 shows the plots of detection percentage versus number of nodes cooperating for three different numbers of averaging values at $SNR = -20$ dB. Figure 28 depicts the effect of number of nodes cooperating on detection percentage at three different SNR values when the number of PSDs averaged is 10. It is difficult to see the effect of the number of nodes on detection percentage at a first glance.

In Figure 27, for the plot of 10 PSDs averaged, a maximum detection percentage is obtained when there are twenty nodes participating in the cooperative wideband spectrum sensing. The second maximum detection percentage value occurs when the participating number of nodes is eight. For the other values of numbers of nodes on this plot, varying detection percentage values are obtained. The reason for this is the positions of the nodes and the applied decision criterion. The positions of Node 8 and Node 20 are (800 m, 500 m) and (1000 m, 600 m), respectively. It can be deduced from Table 5 and Table 6 that these are the two closest nodes to Transmitter 3. When the number of participating nodes is more than eight, Node 8 already participates in spectrum sensing but this time since there are more than eight nodes in the system, the decision criterion requires more nodes observing energy for a particular energy region. Because of these two reasons, the plot of 10 PSDs averaged is not smooth. For higher numbers of PSDs averaged, smoother plots are obtained. This shows that if more PSDs are averaged, the non-smooth effect can be eliminated.
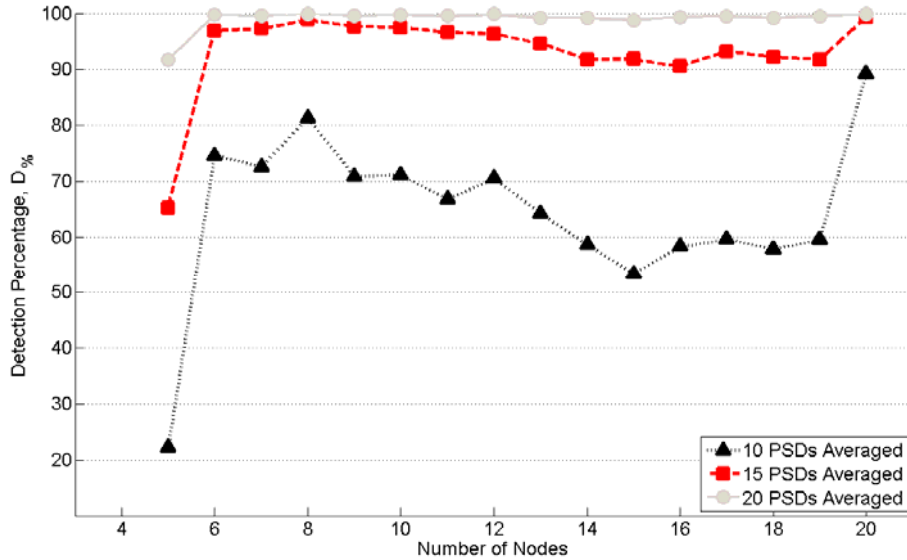
Figure 27.   Detection Percentage versus Number of Nodes for Three Different Number of PSDs Averaged.

As seen in Figure 28, for a particular value of number of nodes, lower detection percentage is obtained when SNR is low. This result is consistent with the results of

Figure 26. Figure 28 also indicates that the non-smooth effect of the positions of the nodes and the applied decision criterion disappears when the SNR is higher.
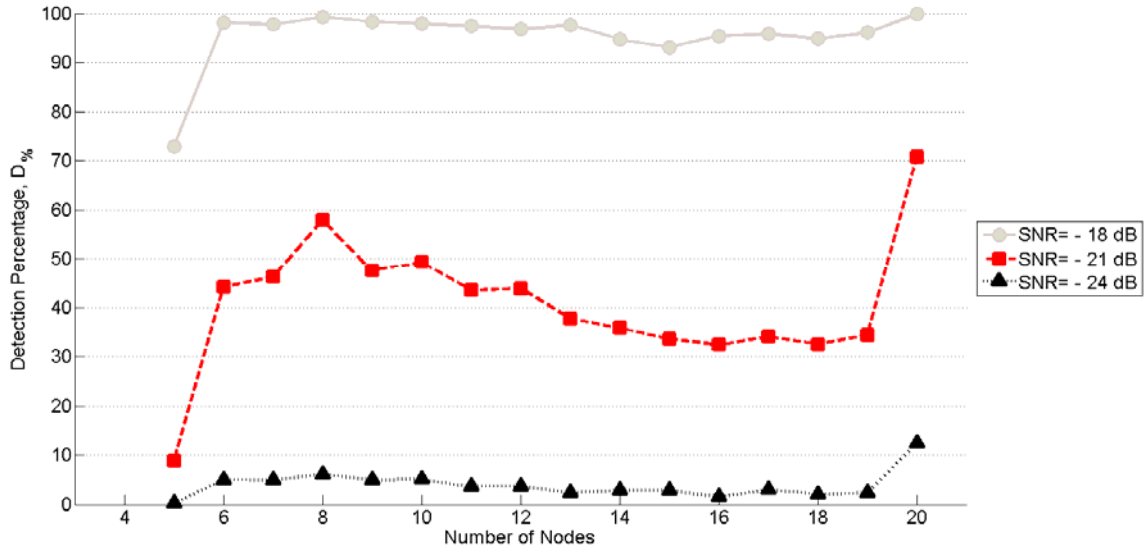
Figure 28.   Detection Percentage versus Number of Nodes for Three Different SNR Values.

4.   Effects of SNR

As mentioned in Chapter III.B, MRSS is a kind of energy detector [9] and the performance of energy detectors depends on the SNR level [8].

Figure 29 shows the effect of SNR on detection percentage for three different number of PSDs averaged values when there are ten nodes participating in cooperative wideband spectrum sensing. Figure 30 shows the plots of detection percentage versus SNR for three different number of node values cooperating when the number of PSDs averaged is ten. Both figures indicate that when the SNR is higher, the proposed scheme performs better in detection.

In Figure 29, for a particular SNR value, when more PSDs are averaged, a higher detection percentage is obtained. This result is consistent with the discussion in [8],

which mentions the need for longer detection time to detect weak signals in energy detectors. When the number of PSDs averaged is increased, it takes more time to decide the presence of the signal of interest.
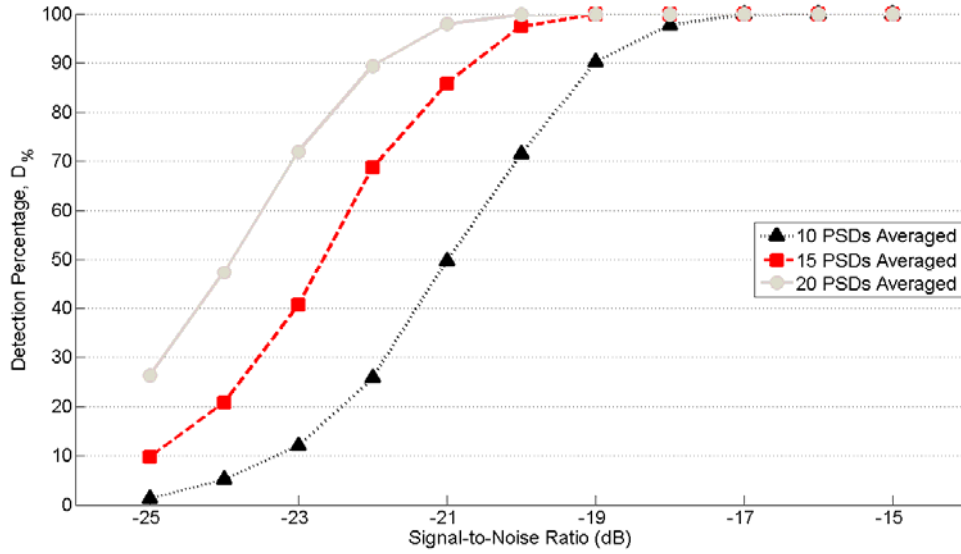
Figure 29.   Detection Percentage versus SNR for Three Different Number of PSDs Averaged.

As explained in Chapter IV.C.3, the positions of the nodes and the applied decision criterion may affect the detection performance and may cause lower detection percentages for higher number of nodes. This effect is also seen in Figure 30. When sixteen nodes cooperate compared to eight and twelve, a lower detection percentage is obtained.
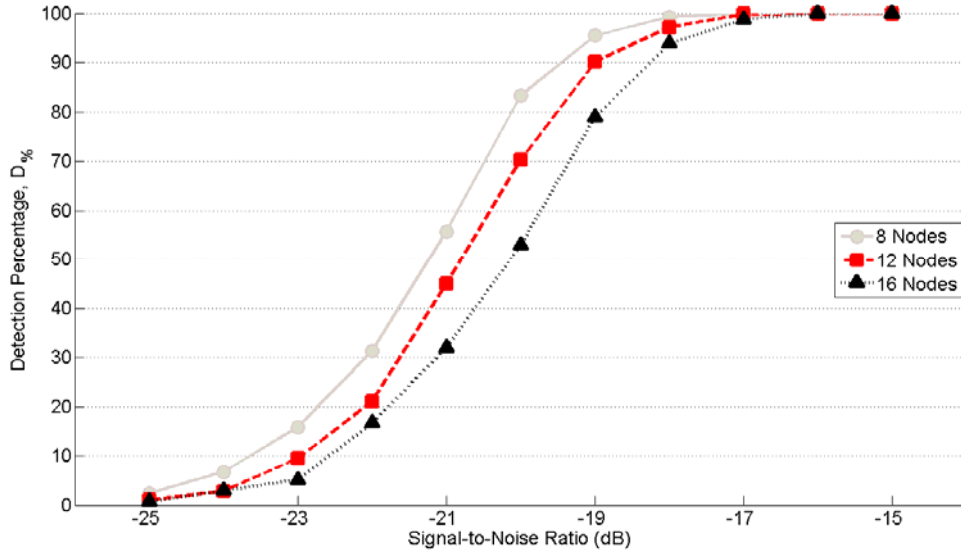
Figure 30.   Detection Percentage versus SNR for Three Different Number of Nodes
Values.

5.   Effect of Number of Transmitters

To evaluate the detection performance of the proposed scheme when there is more than one transmitter in the medium, three different scenarios are considered. Figure 31 shows the performance of the proposed scheme on the detection of the signal emitted by Transmitter 3 for the following scenarios:

1. Only Transmitter 3 is present,

2. Transmitter 1 and Transmitter 3 are present,

3. Transmitter 1, Transmitter 2 and Transmitter 3 are present.

As shown in Figure 31, when other transmitters are present in the medium, percentage of detecting the signal emitted by Transmitter 3 decreases. This is an expected result since the signals of Transmitter 1 and Transmitter 2 contribute to the channel noise while the signal of Transmitter 3 is being detected.
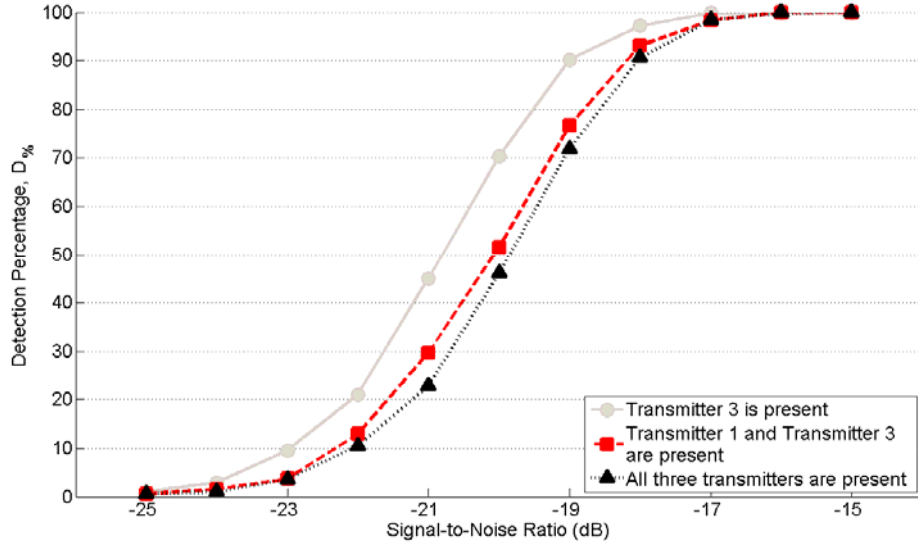
Figure 31.   Detection Percentage of Transmitter 3 versus SNR for Three Different Scenarios.

D.   COMPARISON OF PROPOSED THREE-BIT HARD COMBINATION SCHEME WITH TRADITIONAL HARD COMBINATION SCHEMES

The traditional combination schemes and proposed three-bit hard combination scheme were explained in Chapter III.C. As mentioned in Chapter III.C.1, two of the decision rules used by the traditional hard combination scheme are logical-OR rule and majority rule [28]. This section compares the detection and false alarm performances of the proposed three-bit hard combination scheme and the traditional hard combination schemes using logical-OR rule and majority rule.

In all the simulations of this section, it is assumed that there are 10 nodes participating in the cooperative wideband spectrum sensing, the number of PSDs averaged is 10, σ (standard deviation of the Gaussian variable in the shadowing model) is 10, and the probability of false alarm is 0.1. All results are obtained after 1000 runs of the simulation. When comparing detection performances of the three combination schemes, the detection percentage metric defined in Equation 10 is used, whereas for false alarm performance, the false alarm percentage defined by

$$FA_{\%} = \frac{\text{Number of } f_k \text{ values that give false alarm more than } N_{sim} / 2 \text{ times}}{\text{Round}[(f_{stop} - f_{start}) / f_{sweep}]} \times 100$$

is used, where N_{sim} is the number of simulation runs.

Figure 32 shows the detection percentage versus SNR, for three combination schemes. It shows that when the SNR is between –25 dB and –18 dB, the traditional hard combination schemes have a better detection percentage than the proposed three-bit hard combination scheme. In particular, the traditional hard combination scheme using logical-OR rule is fairly superior to the other two schemes for $SNR < -18$ dB. This is due to the fact that for declaring the presence of the signal of interest, only one node sensing energy above the threshold is enough in a traditional hard combination scheme using logical-OR rule. This fact brings the high detection performance for $SNR < -18$ dB to the traditional hard combination scheme using logical-OR rule. The disadvantage of this fact can be seen when false alarm performances are compared.
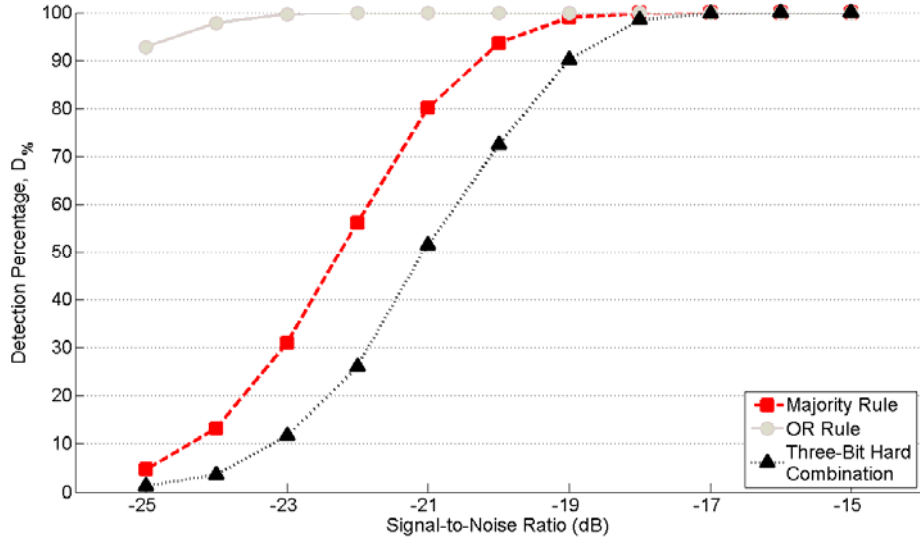
Figure 32.   Detection Percentage versus SNR for Three Combination Schemes.

Figure 33 shows the false alarm performances of the three combination schemes. In particular, the y-axis denotes the percentage of the scanned frequencies in coarse resolution sensing that contributes to false alarm for more than 50% of the simulation.

The x-axis shows the different SNR values. It can be seen from Figure 33 that the proposed three-bit hard combination scheme presents robust false alarm performance compared to the two traditional hard combination schemes. Especially, the fact of sufficiency of only one node sensing energy above the threshold to declare the presence of the signal of interest causes the traditional hard combination scheme using logical-OR rule to present the worst false alarm performance. For example, with the traditional hard combination scheme using logical-OR rule, at $SNR = 10 \, dB$, 62.63% of the scanned frequencies in coarse resolution sensing will be sent to the fine resolution sensing block redundantly.
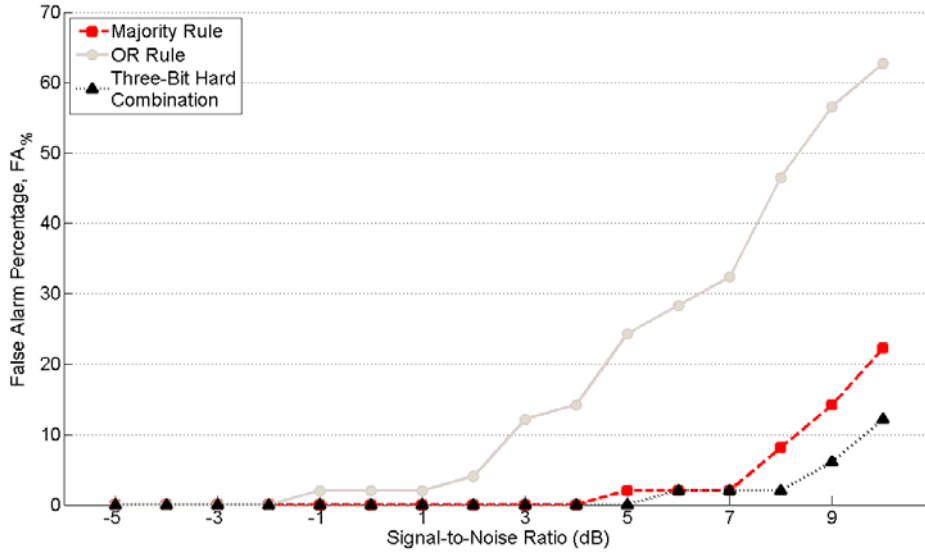
Figure 33.   False Alarm Percentage versus SNR for Three Combination Schemes.

When the results of Figure 32 and Figure 33 are analyzed, the following conclusions can be made. The higher percentage of the scanned frequencies in coarse resolution sensing that contribute to false alarms means that some of the nodes will apply fine resolution sensing unnecessarily. This is a waste of scarce battery energy for redundant computations and communications between the node and the decision maker. As mentioned in Chapter IV.C.2, the detection performance of the three-bit hard combination scheme can easily be improved by increasing the number of PSDs averaged. Increasing the number of PSDs averaged requires more computations, but the cost of

these excess computations is less than the cost of the communication overload, which requires more battery power in wireless sensor networks [37]. Because of this, even the traditional hard combination using logical-OR rule presents better detection performance for conditions where $\text{SNR} < -18 \text{ dB}$; proposed three bit combination scheme is more convenient for the RF sensor networks considered in this thesis.

E.   RSS-BASED LOCALIZATION RESULTS

This section presents the simulation results of RSS-based localization [5] used in the localization part of the proposed sensor network based cooperative wideband spectrum sensing and localization scheme. To evaluate the performance of the RSS-based localization scheme, mean square error (MSE) for position and the average absolute power estimation error (PEE) are used. MSE is defined as

$$\xi_{MSE} = \frac{1}{N_{sim}} \sum_{n=1}^{N_{sim}} \sqrt{(x - x_{est,n})^2 + (y - y_{est,n})^2}$$

where (x, y) is the true position of the transmitter, $(x_{est,n}, y_{est,n})$ is the nth position estimation, N_{sim} is the number of simulation runs. PEE is defined as

$$\xi_{PEE} = \frac{1}{N_{sim}} \sum_{n=1}^{N_{sim}} \left| P_t - P_{est,n} \right|$$

where P_t is the true EIRP of the transmitter and $P_{est,n}$ is the nth EIRP estimation. In particular, the effects of number of samples, number of nodes, and σ (standard deviation of the Gaussian random variable used in the shadowing model) on the above error parameters are studied.

Localization simulation is applied to estimate the position and EIRP of Transmitter 3. All results are obtained by running the simulation 10,000 times and averaging the results. As mentioned in Chapter IV.B.2.b, it is assumed that C_j constants representing the factors affecting the RSS values at j^{th} node are chosen as 1, path loss

exponent α is 3, and node positions are as shown in Table 6. It is further assumed that the EIRP of Transmitter 3 is 1 W and its position is (1500 m, 1100 m) as given in Table 5.

1. Effects of Number of Samples

As explained in Chapter IV.B.2.a, every node samples RSS values R times and takes the average of these values to minimize the unwanted effect of shadowing.

Figure 34 shows the plots of the position estimation MSE versus number of samples for different number of nodes values with $\sigma = 3$. Figure 35 depicts the effect of the number of samples on position estimation MSE for different values of σ when there are five nodes participating in the localization process. Both Figure 34 and Figure 35 indicate that when the number of samples R is increased, the error in position estimation decreases. This is an expected result because when the number of samples is increased, the unwanted effect of shadowing decreases and the localization scheme produces better estimations. In both figures, the rate of decrease in position error reduces when the number of samples increases.

In Figure 34, for a particular value of number of samples, when the number of nodes participating in the localization process is increased from five to ten, position estimation MSE decreases dramatically, whereas an increase from ten nodes to fifteen nodes does not provide a remarkable improvement in position estimation MSE.

Figure 34.   Position Estimation MSE versus Number of Samples for Three Different Numbers of Nodes with $\sigma = 3$.

In Figure 35, for a particular number of samples, when the σ increases, the error in position estimation also increases.   This is an expected result, because higher σ implies a severe shadowing effect.
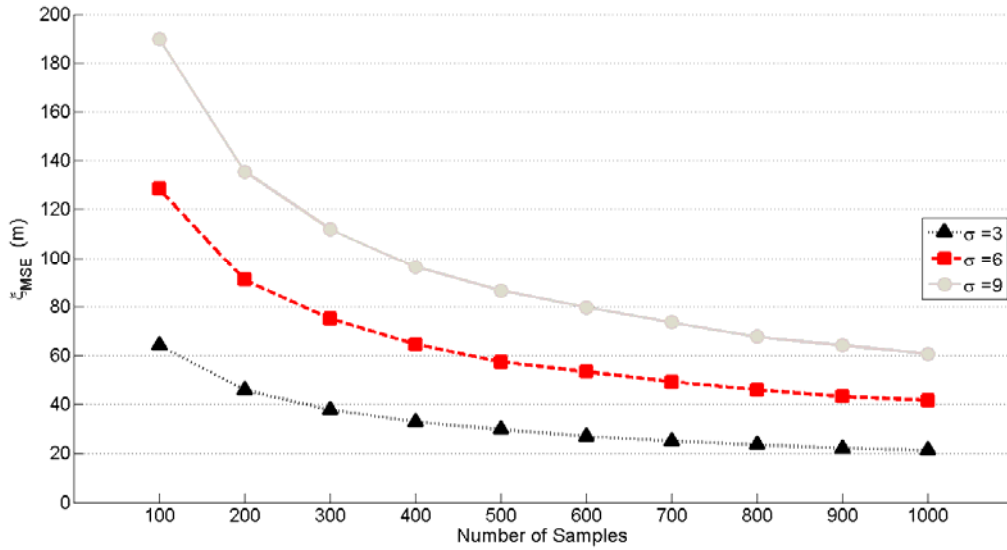
Figure 35.   Position Estimation MSE versus Number of Samples for Three Different σ Values when Five Nodes Participate in Localization.

Figure 36 and Figure 37 show the effects of number of samples on average absolute power estimation error for different values of number of nodes and standard deviation σ, respectively. Both graphs present the same effects seen on Figure 34 and Figure 35, as explained above. In particular, the average absolute power estimation error decreases when the number of samples is increased. For a particular number of samples value, when the number of nodes is increased or the standard deviation σ is reduced, lower estimation error occurs.

Figure 36.   Average Absolute Power Estimation Error versus Number of Samples for Three Different Number of Nodes with $\sigma = 3$.

Figure 37.   Average Absolute Power Estimation Error versus Number of Samples for Three Different σ Values when Five Nodes Participate in Localization.

2.   Effects of Number of Nodes

It was mentioned in Chapter IV.C.3 that because of limited battery power or environmental effects, sensor nodes can fail in wireless sensor networks [36]. Since sensor nodes collaborate in the proposed scheme, the number of nodes participating in localization affects the localization performance.

Figure 38 depicts the plots of the position estimation MSE versus number of nodes for different values of number of samples when $\sigma = 3$. Figure 39 shows the effect of the number of nodes on position estimation MSE for different values of σ when the number of samples is 200. Both Figure 38 and Figure 39 show that even though there are small fluctuations in the plots, when the number of nodes participating in the localization process increases, the error in position and power estimations decreases. The fluctuations in the plots are due to the positions of the nodes as explained in Chapter IV.C.3.

In Figure 38, it can be seen that for a given number of nodes value, when more samples are used to determine the averaged RSS value, the error in position estimation decreases.
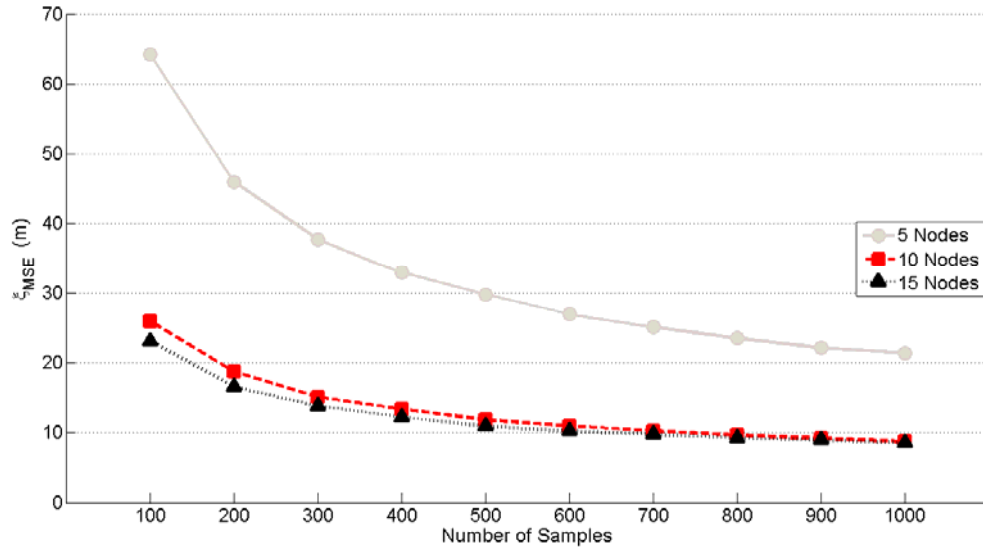
66
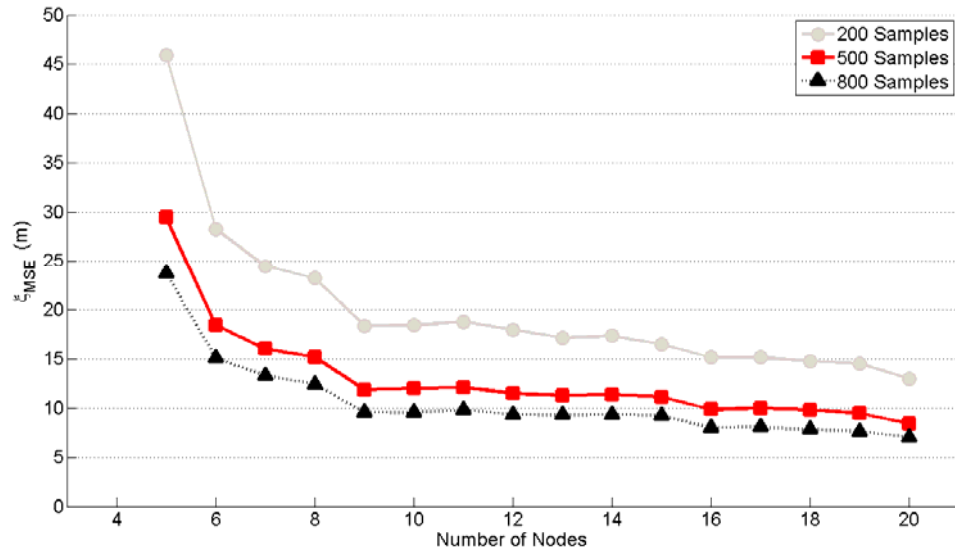
Figure 38.   Position Estimation MSE versus Number of Nodes for Three Different Numbers of Samples with $\sigma = 3$.

In Figure 39, for a specific number of nodes value, a higher σ worsens the shadowing effect and increases the error in position estimation.
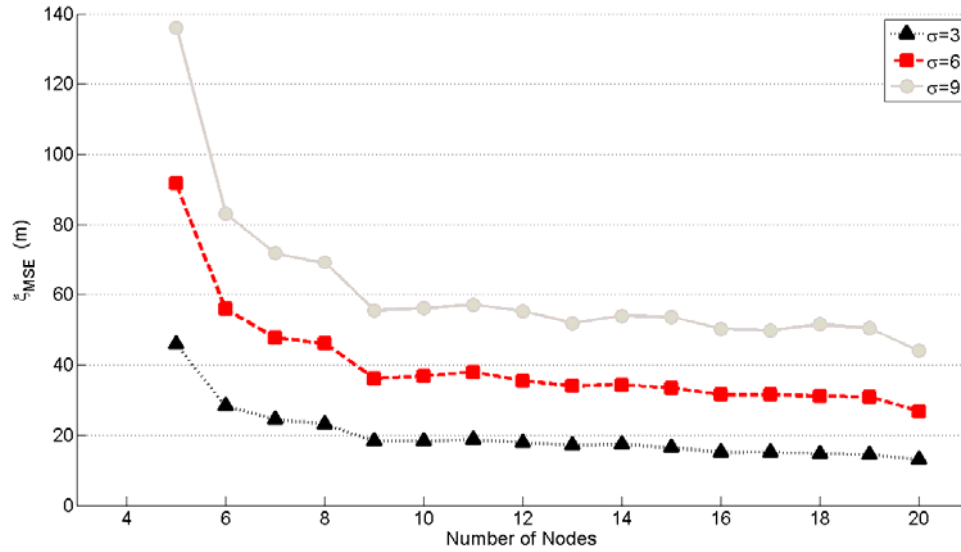
Figure 39.   Position Estimation MSE versus Number of Nodes for Three Different σ Values when the Number of Samples is 200.

Figure 40 and Figure 41 show the effects of number of nodes on average absolute power estimation error for different values of number of samples and standard deviation σ, respectively. Both graphs present the same effects seen in Figure 38 and Figure 39. In particular, the average absolute power estimation error decreases when the number of nodes is increased. For a particular number of nodes value, when the number of samples is increased or standard deviation σ is decreased, estimation error decreases.
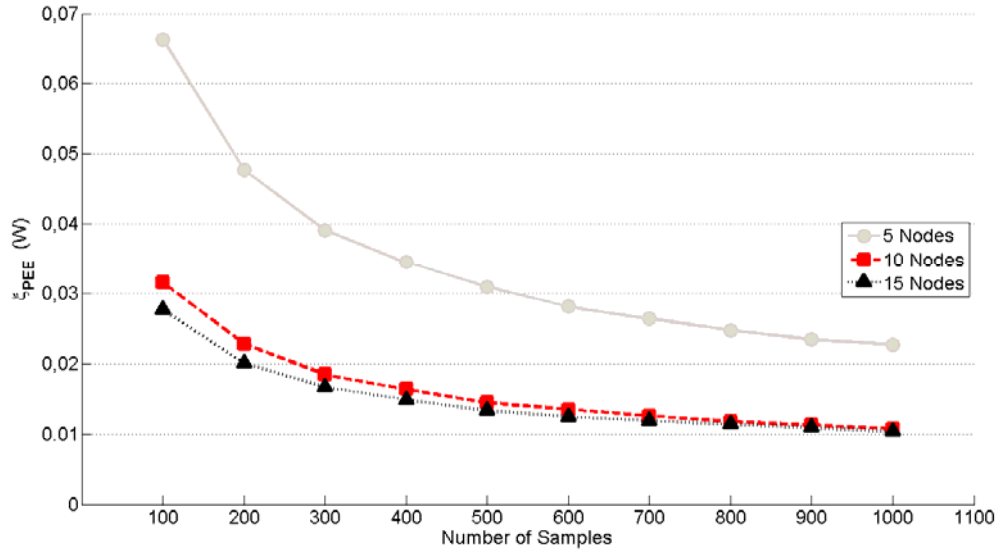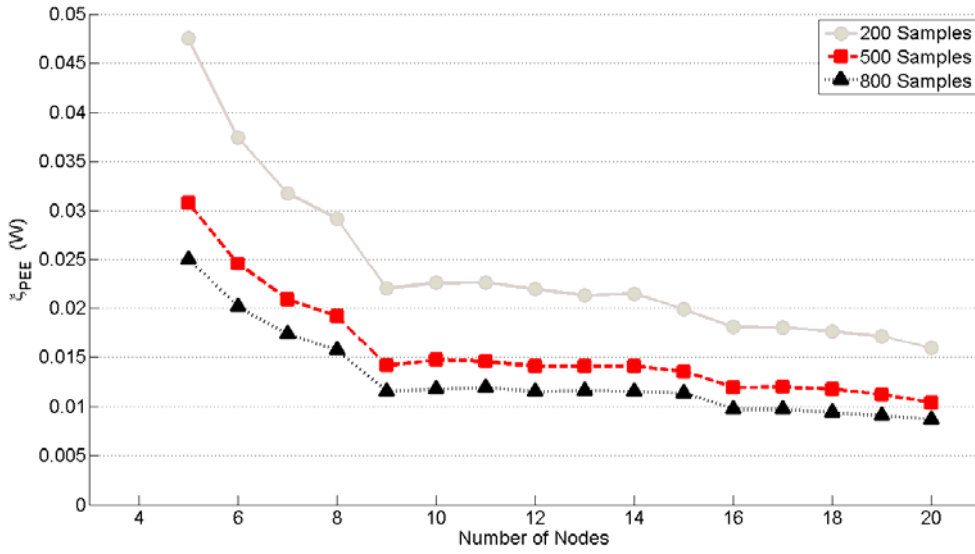

Figure 40.   Average Absolute Power Estimation Error versus Number of Nodes for Three Different Numbers of Samples with $\sigma = 3$.
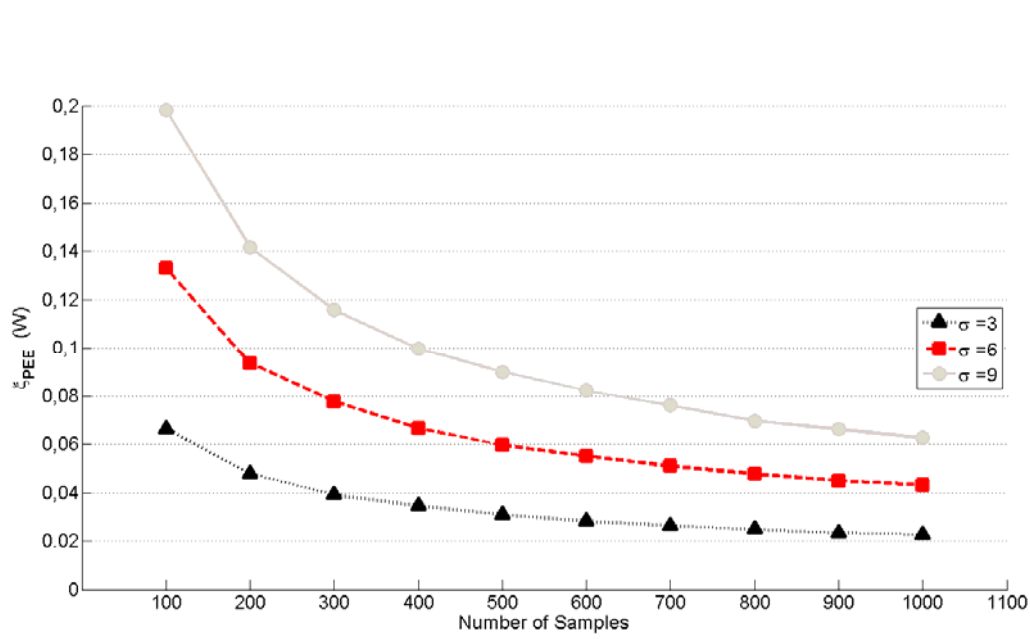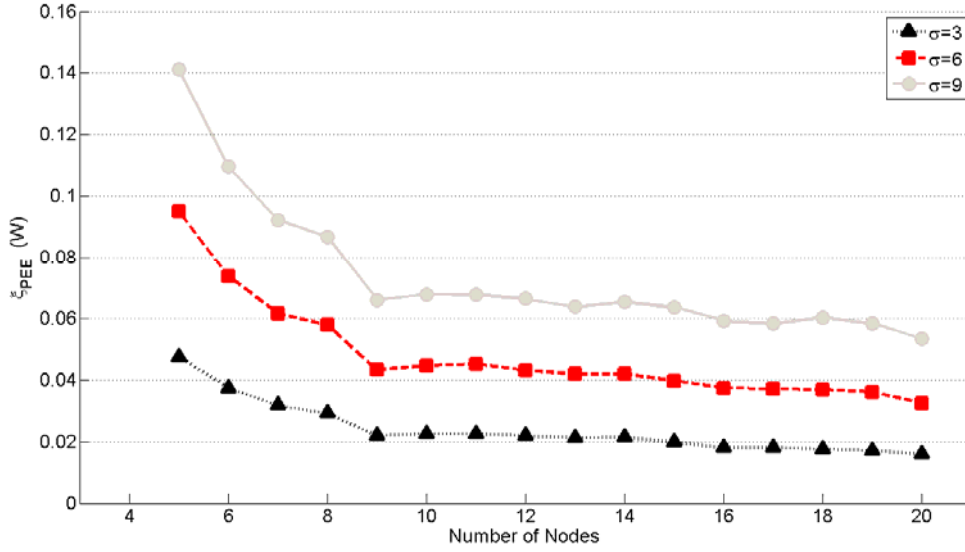
Figure 41.   Average Absolute Power Estimation Error versus Number of Nodes for Three Different σ Values when the Number of Samples is 200.

3.   Effects of σ

Shadowing affects measured RSS values [5]. As mentioned in Chapter IV.B.2.a, a log-normal path loss model is used to include the shadowing effect. Standard deviation of the Gaussian variable σ in Equation 8 determines the level of the shadowing effect.

Figure 42 depicts plots of the position estimation MSE versus σ for different values of the number of samples in RSS averaging when there are five nodes participating in the localization process. Figure 43 shows the effects of σ on position estimation MSE for different numbers of nodes participating in the localization process when the number of samples is 200. Both Figure 42 and Figure 43 show that when σ increases, the shadowing effect becomes severe and the error in position estimation increases.

In Figure 42, it can be seen that for a given σ value, when the number of samples is increased, the disturbance caused by the shadowing effect is reduced and error in position estimation decreased.
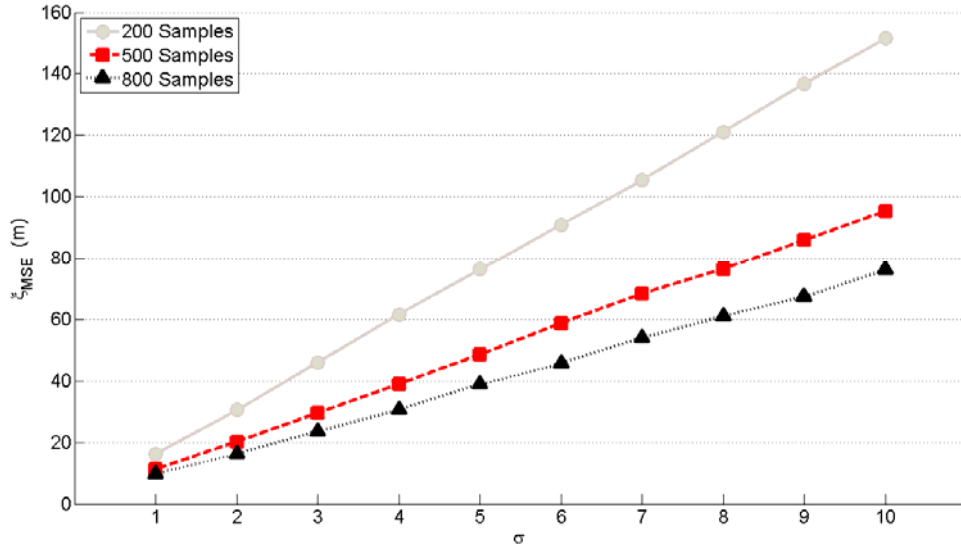
Figure 42.   Position Estimation MSE versus σ for Three Different Numbers of Samples when Five Nodes Participate in Localization.

Figure 43 shows that for a given σ value, when the number of nodes participating in the localization process increases from five to ten, the position estimation MSE decreases dramatically, whereas an increase from ten nodes to fifteen nodes does not provide a remarkable improvement in position estimation MSE.
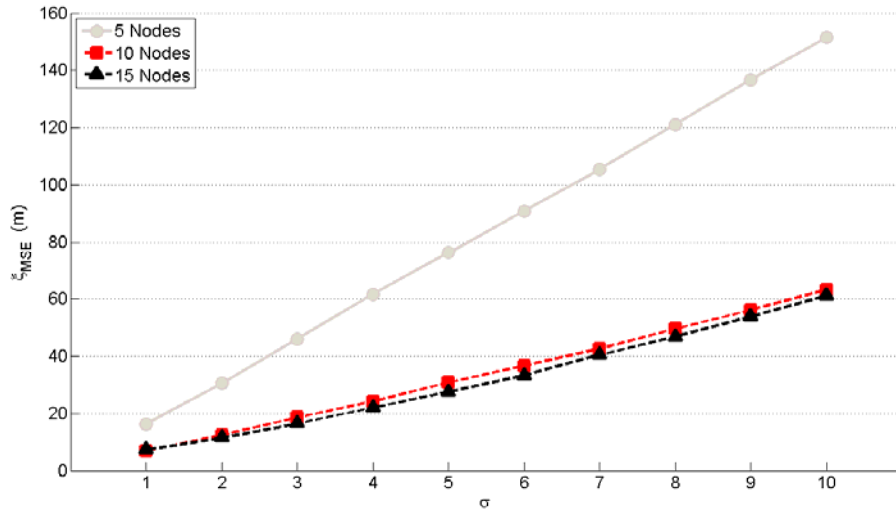
Figure 43.   Position Estimation MSE versus σ for Three Different Numbers of Nodes when the Number of Samples is 200.

Figure 44 and Figure 45 show the effects of σ on average absolute power estimation error for different values of number of samples and number of nodes, respectively. Both graphs present the same effects seen in Figure 42 and Figure 43, explained above. In particular, the average absolute power estimation error increases when standard deviation σ increases. For a given σ value, an increase in the number of samples or the number of nodes decreases the average absolute power estimation error.
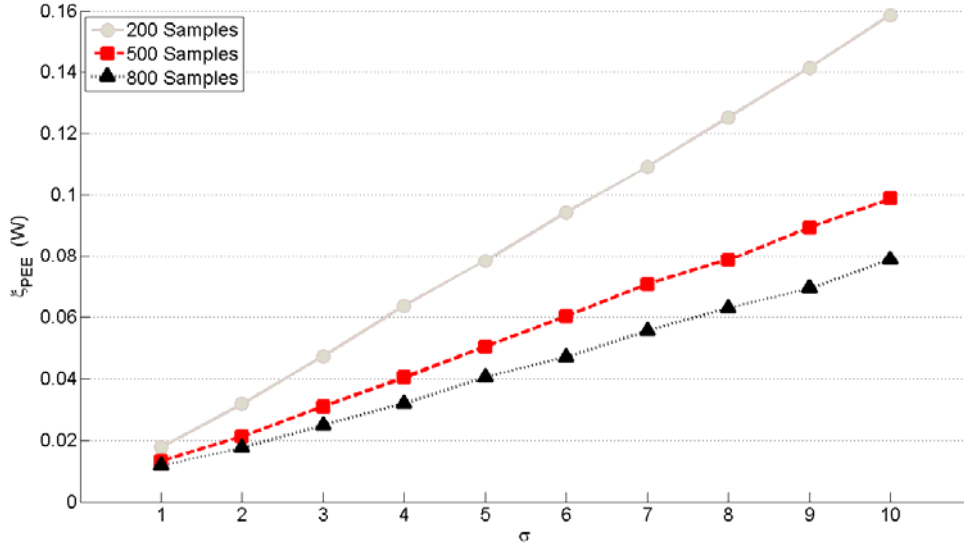
Figure 44.   Average Absolute Power Estimation Error versus σ for Three Different
Numbers of Samples when Five Nodes Participate in Localization.
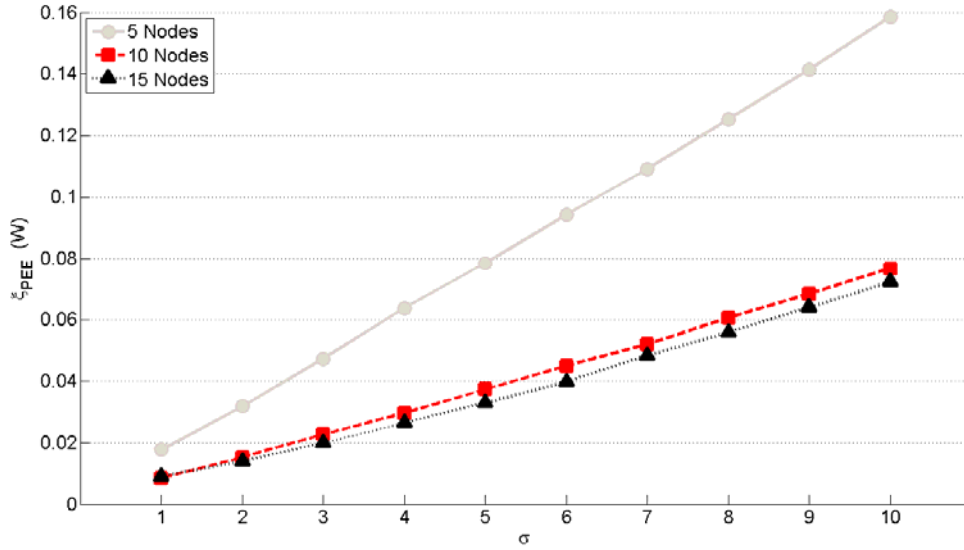
Figure 45.   Average Absolute Power Estimation Error versus σ for Three Different Numbers of Nodes when Number of Samples is 200.

F.   INSTANTANEOUS ESTIMATION RESULTS

In previous sections of this chapter, the results presented for the proposed sensor network based cooperative wideband spectrum sensing and localization scheme were based on a large number of simulation runs (1000 or 10000). This section presents instantaneous results of the proposed scheme. The results are based on a small number, specifically one and five simulation runs.

Figure 46 shows the result of cooperative wideband spectrum sensing applied by 12 nodes when the probability of false alarm is 0.1, SNR is –9 dB, σ is 10, and other parameters are as assumed in Chapter IV.B.1. As can be seen from Figure 46, nodes are able to detect Transmitter 2 and Transmitter 3. Since the distances between Transmitter 1 and the nodes are greater, Transmitter 1 cannot be detected.
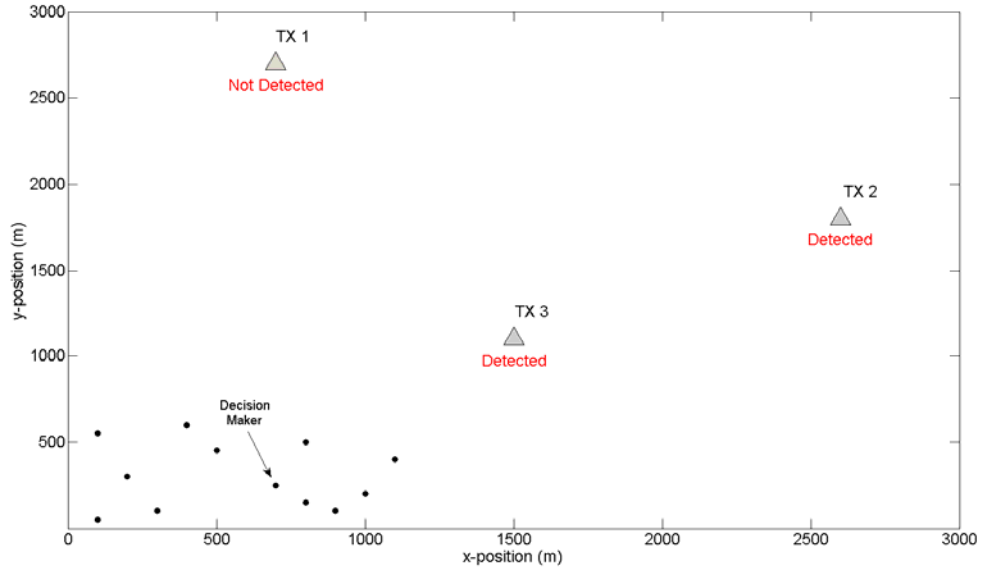
Figure 46.   Instantaneous Estimation Result of Cooperative Wideband Spectrum Sensing with 12 Nodes when $p_{FA} = 0.1$, SNR $= -9$ dB, and $\sigma = 10$.

Figure 47 shows the power and position estimations of RSS-based localization applied by 12 nodes with $\sigma = 10$, $\alpha = 3$, $M = 500$, and other parameters as assumed in Chapter IV.B.2. Transmitters have the specifications listed in Table 5. Five position estimations of each transmitter are shown with crosses. To minimize the clutter in the figure, only one power estimation value for each transmitter is shown in Figure 47. As can be seen from this figure, since Transmitter 3 is closer than the other two transmitters, position estimations for this transmitter are more precise.
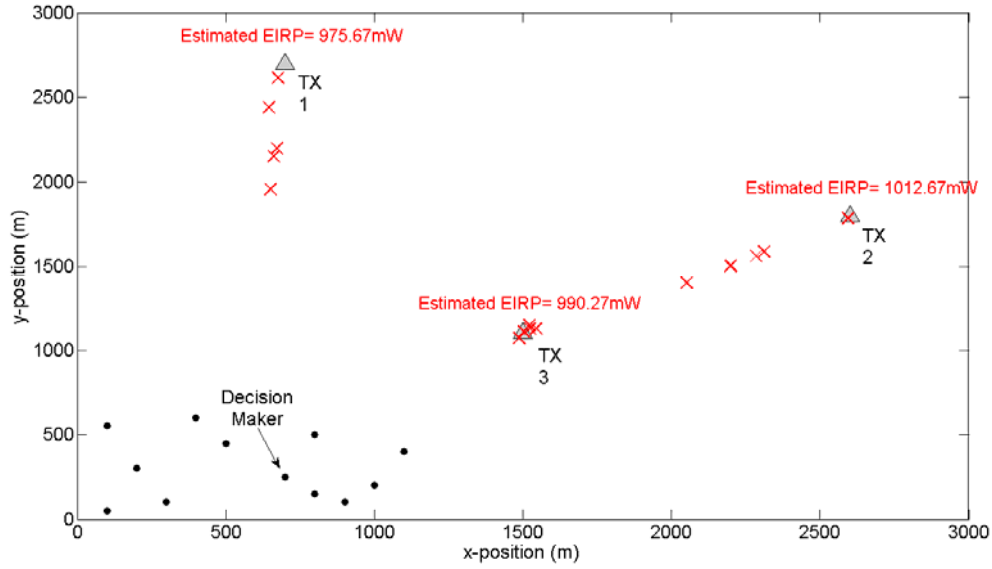
Figure 47.   EIRP and Position Estimations of RSS-based Localization Scheme with 12 Nodes when $\sigma =10$, $\alpha =3$ and $M =500$.

G.   SUMMARY

This chapter presented the simulation model developed to implement the proposed scheme, and the simulation results. Firstly, coarse and fine resolution sensing results for a node were illustrated.   For cooperative wideband spectrum sensing, simulation results showing the effects of the window type on detection margin, the effects of number of PSDs averaged, number of nodes, SNR, and number of transmitters on the detection percentage of the cooperative wideband spectrum sensing part of the proposed scheme were illustrated.   Simulation results comparing the proposed three-bit hard combination scheme with traditional hard combination schemes were also presented.

For RSS-based localization, simulation results showing the effects of number of samples, number of nodes, and σ (standard deviation of the Gaussian variable in the shadowing model) on mean square error of position estimation and average absolute power estimation error were illustrated.   Lastly, instantaneous estimation results of cooperative wideband spectrum sensing and RSS-based localization were presented.

V.   CONCLUSIONS

This thesis focused on spectrum sensing and localization with radio frequency (RF) sensor networks. An RF sensor network can be deployed over an area of interest to detect the signals in the air, to determine the frequencies of these signals, and to estimate the positions and effective isotropic radiated powers (EIRPs) of the transmitters emitting these signals. Maximizing the signal detection performance and the accuracy of position and power estimations with a minimal computation complexity is an additional objective.

A.   SUMMARY OF THE WORK DONE

To meet these objectives, a sensor network based cooperative spectrum sensing and localization scheme was proposed. Wavelet-based multi-resolution spectrum sensing (MRSS) [4] and received signal strength (RSS)-based localization [5] methods, which were originally proposed for cognitive radio applications, were adapted to RF sensor networks to implement spectrum sensing and localization. A new three-bit hard combination technique was proposed for cooperation of the nodes. A simulation model was developed in MATLAB programming language to implement the proposed scheme and to analyze its simulation performance. Different window types, number of power spectral densities (PSDs) averaged, number of nodes, signal-to-noise-ratio (SNR) values, and number of transmitters were simulated to analyze the effects on the detection performance of the cooperative wideband spectrum sensing part of the proposed scheme. Comparison of the three-bit hard combination scheme and the traditional hard combination schemes were also presented. Different values of number of samples, number of nodes, and standard deviation of the Gaussian variable in the shadowing model were simulated to analyze the effects on the performance of the localization part of the proposed scheme.

B.   SIGNIFICANT RESULTS

The proposed sensor network based cooperative wideband spectrum sensing and localization scheme is appropriate for RF sensor networks since it senses a wide spectrum

band in an energy efficient manner by providing resilience to fading, shadowing, and noise. Energy efficiency comes from the usage of MRSS and the proposed three-bit hard combination scheme. In particular, redundant exhaustive sensing on empty bands is avoided with MRSS, and less overhead in collaboration with respect to the soft combination is provided by three-bit hard combination. RSS-based localization provides the location and EIRP of the source of interest. Resilience to fading, shadowing, and noise is due to the cooperation of the nodes.

Results of the cooperative spectrum sensing part of the proposed scheme showed that using rectangular window in MRSS provides the highest detection margin. The positions of the nodes participating in the sensing process and the applied decision criterion affect the detection performance.

The proposed three-bit hard combination scheme is superior to the traditional hard combination schemes in false alarm reduction. The detection performance of the three-bit hard combination scheme can be improved with little additional cost by increasing the number of averaged PSDs.

The simulation results of the localization part of the proposed scheme showed that average absolute power estimation error presents the same behavior as the position estimation error. In particular, these two error metrics are affected in a similar manner by the number of samples, number of nodes, and standard deviation of the Gaussian variable in the shadowing model.

C.   FUTURE WORK

There are several ideas for future work from this thesis. First, simulation models can be improved. Multipath fading effects could be added and their effects on the performance of the proposed scheme could be investigated. Instead of generating the RF signals in MATLAB, actual transmitted signals could be collected in the field. The proposed three-bit hard combination scheme could be compared with the two-bit hard combination scheme. In the simulation results, probability of detection could be illustrated as a detection performance measure.

The three-bit hard combination scheme could be improved. In weight determination, optimal values for the percentage of nodes required in a given region to declare the presence of the signal of interest could be determined using detection theory. Different weights for the energy observation regions, and different decision criteria could be studied and their effect on the performance of the proposed scheme could be analyzed. Thresholds could be determined to satisfy the target overall false alarm probability of the M-node network [6].

For the localization part of the proposed scheme, RSS measurements and sensor node positions were assumed to be given. This assumption is a drawback of the proposed scheme and the following ideas are offered for a future study. RSS measurements could be implemented using a received signal strength indicator circuit. Node positions could be determined using a range-free localization scheme.

THIS PAGE INTENTIONALLY LEFT BLANK

APPENDIX

The appendix contains selected MATLAB code used to evaluate the performance of the proposed sensor network based cooperative wideband spectrum sensing and localization scheme.

A. CODE USED TO STUDY THE EFFECT OF NUMBER OF NODES ON DETECTION PERCENTAGE OF THE COOPERATIVE WIDEBAND SPECTRUM SENSING PART OF THE PROPOSED SCHEME

This code was used to generate the curve for $\text{SNR}=-18\text{ dB}$ in Figure 28.

```
%Volkan Sonmezer, Sep 2009, Naval Postgraduate School, Monterey,CA, USA

%This code is used to study the effect of number of nodes on detection
performance of the cooperative wideband spectrum sensing part of the
proposed scheme.

clc
clear all


%%%%%%%%%%%%%%%%%%%%          PARAMETERS FOR MRSS     %%%%%%%%%%%%%%%%%%%%%%
fstart=31e6;        %We examine the spectrum between 31MHz and 130MHz
fstop=130e6;

fs=1e9;             %Sampling Frequency is 1GHz for all nodes
ts=1/fs;

fsweep_c=5e6;       %Sweeping frequency for central node
Tw_c=0.1e-6;        %Window Length value for central node
s_length_c=Tw_c;
win_c=rectwin(Tw_c/ts);      %Rectangular window is applied
t_int_c=(0:ts:Tw_c-ts)';     %Integral interval is Tw

fsweep=2e6;                  %Sweeping frequency for other nodes
Tw=2e-6;                     %Window Length value for other nodes
s_length=Tw;
win=rectwin(Tw/ts);          %Rectangular window is applied
t_int=(0:ts:Tw-ts)';         %Integral interval is Tw

%%%%%%%%%%    GENERATION OF 16QAM SIGNAL FOR CENTRAL NODE    %%%%%%%%%%
fc3=95e6;                %Frequency of the 16-QAM  signal
A = 16;                  %Alphabet size
rand('state',0)          %To stabilize the power of the incoming signal
x3_c = randint(s_length_c*fs,1,A);       %Random digital message
opt_c=randint(s_length_c*fs,1,A);
s3_0_c=modulate(x3_c,fc3,fs,'qam',opt_c); %QAM Modulation
```

```matlab
%%%%%%%%%%   GENERATION OF 16QAM SIGNAL FOR OTHER NODES   %%%%%%%%%%
fc3=95e6;                    %Frequency of the 16-QAM  signal
A = 16;                      %Alphabet size
rand('state',0)              %To stabilize the power of the incoming signal
x3 = randint(s_length*fs,1,A);     %Random digital message
opt=randint(s_length*fs,1,A);
s3_0=modulate(x3,fc3,fs,'qam',opt); %QAM Modulation


%%%%%%%%%%%%%%%%%%%         VARIABLE PARAMETERS      %%%%%%%%%%%%%%%%%%%%%
N=10;        %Number of PSDs averaged
N_c=N*1;     %Number of PSDs averaged for central nodes
SNR=-18;     %SNR in dB
L=1000;      %Number of Simulation Runs
PFA=0.1;     %Probability of False Alarm Value
sigma=10;    %Standard Deviation of the Gaussian Var. in Shadowing Model


ss=0;        %Dummy variable


%%%%%%%%%%%%%%%%%%%%%%%%%%%%%%%%%%%%%%%%%%%%%%%%%%%%%%%%%%%%%%%%%%%%%%%%%%%
    %FINDING THE DETECTION PERCENTAGE FOR DIFFERENT NUMBER OF NODES
%%%%%%%%%%%%%%%%%%%%%%%%%%%%%%%%%%%%%%%%%%%%%%%%%%%%%%%%%%%%%%%%%%%%%%%%%%%


for M=5:1:20

    %%% Preallocation of matrices to increase the calculation speed %%%
    zI=zeros(N,ceil((fstop-fstart+1)/fsweep));
    zQ=zeros(N,ceil((fstop-fstart+1)/fsweep));
    nnI=zeros(N,ceil((fstop-fstart+1)/fsweep));
    nnQ=zeros(N,ceil((fstop-fstart+1)/fsweep));
    R=zeros(M,ceil((fstop-fstart+1)/fsweep));
    H1=zeros(1,ceil((fstop-fstart+1)/fsweep));
    zI_c=zeros(N_c,ceil((fstop-fstart+1)/fsweep_c));
    zQ_c=zeros(N_c,ceil((fstop-fstart+1)/fsweep_c));
    nnI_c=zeros(N_c,ceil((fstop-fstart+1)/fsweep_c));
    nnQ_c=zeros(N_c,ceil((fstop-fstart+1)/fsweep_c));

    ss=ss+1;

    for Sim=1:L     %Beginning of L times run

%%%%%%%%%%%%%%%%%%%%%%%%%%%%%%%%%%%%%%%%%%%%%%%%%%%%%%%%%%%%%%%%%%%%%%%%%%%%
            %THRESHOLD DETERMINATION BY CENTRAL NODE (Node 1)
%%%%%%%%%%%%%%%%%%%%%%%%%%%%%%%%%%%%%%%%%%%%%%%%%%%%%%%%%%%%%%%%%%%%%%%%%%%%

        %Adjusting the signal power values at the Central Node (Node 1)
        s3_1_c=4.9728e-6*s3_0_c;   %Signal with power value=-92.02 dB

        for m=1:N_c  %Calculating the PSD for every frequency N_c times

            %Generating Shadowing effect for 16-QAM signal
            xi=normrnd(0,sigma);
            s3_2_c=10^(-xi/200)*s3_1_c;
```

```matlab
    %Adding Channel Noise to provide given SNR
    s_c=s3_2_c;
    si_c= awgn(s3_2_c,SNR,'measured','dB');

%Adding the effect of LNA gain which is 40dB and thermal noise
    Tnoise_c=wgn(s_length_c*fs,1,-88.98);
    r_c=si_c*100+Tnoise_c; %Signal at the output of the LNA

    %Calculation of the Total Noise
    noise1_c =100*(si_c-s_c);        %AWGN Channel Noise
    noise2_c=Tnoise_c;               %Thermal Noise
    noise_c=noise1_c+noise2_c;

    n=1;   %n is the index for frequency value

    %Sweeping the spectrum
    %(Look at analog correlation part of the MRSS diagram)
    for fk=fstart:fsweep_c:fstop
        wI_c=win_c.*cos(2*pi*fk*t_int_c);
        yI_c=r_c.*wI_c;
        nI_c=noise_c.*wI_c;
        zI_c(m,n)=(1/Tw_c)*trapz(t_int_c,yI_c);
        nnI_c(m,n)=(1/Tw_c)*trapz(t_int_c,nI_c);
        wQ_c=win_c.*sin(2*pi*fk*t_int_c);
        yQ_c=r_c.*wQ_c;
        nQ_c=noise_c.*wQ_c;
        zQ_c(m,n)=(1/Tw_c)*trapz(t_int_c,yQ_c);
        nnQ_c(m,n)=(1/Tw_c)*trapz(t_int_c,nQ_c);
        n=n+1;
    end
end

%Averaging the PSDs for signal plus noise input
zI_avg_c=sum(zI_c)/N_c;
zQ_avg_c=sum(zQ_c)/N_c;

%Averaging the PSDs for noise only input
nnI_avg_c=sum(nnI_c)/N_c;
nnQ_avg_c=sum(nnQ_c)/N_c;

%We find the statistics of the normal distribution that fits
%to the noise input of the envelope detector
[mu,sigma]=normfit(nnI_avg_c);

%Parameters of the Weibull distribution
a=sqrt(2)*sigma;
b=2;

%Numeric threshold values
T1_0=wblinv(1-PFA,a,b);
T2_0=wblinv(1-0.1*PFA,a,b);
T3_0=wblinv(1-1e-2*2*PFA,a,b);
T4_0=wblinv(1-1e-3*3*PFA,a,b);
T5_0=wblinv(1-1e-4*4*PFA,a,b);
```

```matlab
        T6_0=wblinv(1-1e-5*5*PFA,a,b);
        T7_0=wblinv(1-1e-6*6*PFA,a,b);


        %Threshold values in dB
        T1=10*log10(T1_0);
        T2=10*log10(T2_0);
        T3=10*log10(T3_0);
        T4=10*log10(T4_0);
        T5=10*log10(T5_0);
        T6=10*log10(T6_0);
        T7=10*log10(T7_0);


%%%%%%%%%%%%%%%%%%%%%%%%%%%%%%%%%%%%%%%%%%%%%%%%%%%%%%%%%%%%%%%%%%%%%%%%
        %APPLICATION OF COARSE RESOLUTION SENSING AT OTHER NODES
%%%%%%%%%%%%%%%%%%%%%%%%%%%%%%%%%%%%%%%%%%%%%%%%%%%%%%%%%%%%%%%%%%%%%%%%

        for k=2:M        %There are 19 Nodes other than the central node

            %Adjusting RSS values at every node
            switch (k)
                case 2
                %16QAM Signal at Node 2
                s3_1=4.984e-6*s3_0; %Signal with power value=-101.43dB
                case 3
                %16QAM Signal at Node 3
                s3_1=6.0059e-6*s3_0;
                case 4
                %16QAM Signal at Node 4
                s3_1=3.2142e-6*s3_0;
                case 5
                %16QAM Signal at Node 5
                s3_1=3.3272e-6*s3_0;
                case 6
                %16QAM Signal at Node 6
                s3_1=8.6712e-6*s3_0;
                case 7
                %16QAM Signal at Node 7
                s3_1=4.8148e-6*s3_0;
                case 8
                %16QAM Signal at Node 8
                s3_1=7.0889e-6*s3_0;
                case 9
                %16QAM Signal at Node 9
                s3_1=3.4e-6*s3_0;
                case 10
                %16QAM Signal at Node 10
                s3_1=4.7204e-6*s3_0;
                case 11
                %16QAM Signal at Node 11
                s3_1=2.707565e-6*s3_0;
                case 12
                %16QAM Signal at Node 12
                s3_1=4.8874e-6*s3_0;
                case 13
                %16QAM Signal at Node 13
```

```matlab
            s3_1=4.014e-6*s3_0;
        case 14
        %16QAM Signal at Node 14
            s3_1=3.1519e-6*s3_0;
        case 15
        %16QAM Signal at Node 15
            s3_1=2.9415e-6*s3_0;
        case 16
        %16QAM Signal at Node 16
            s3_1=4.94389e-6*s3_0;
        case 17
        %16QAM Signal at Node 17
            s3_1=7.08058e-6*s3_0;
        case 18
        %16QAM Signal at Node 18
            s3_1=3.4164e-6*s3_0;
        case 19
        %16QAM Signal at Node 19
            s3_1=6.26713e-6*s3_0;
        case 20
        %16QAM Signal at Node 20
            s3_1=10.54554e-6*s3_0;
    end

    for m=1:N  %Calculating the PSD for every frequency N times

        %Generating the shadowing effect for 16QAM signal
        xi=normrnd(0,sigma);
        s3_2=10^(-xi/200)*s3_1;

        %Adding channel noise to provide given SNR
        s=s3_2;
        si=awgn(s3_2,SNR,'measured','dB');

%Adding the effect of LNA gain which is 40dB and thermal noise
        Tnoise=wgn(s_length*fs,1,-101.99);
        r=si*100+Tnoise; %Signal at the output of the LNA

        n=1;    %n is the index for frequency value

        %Sweeping the spectrum
        %(Look at the analog correlation part of the MRSS)
        for fk=fstart:fsweep:fstop
            wI=win.*cos(2*pi*fk*t_int);
            yI=r.*wI;
            zI(m,n)=(1/Tw)*trapz(t_int,yI);
            wQ=win.*sin(2*pi*fk*t_int);
            yQ=r.*wQ;
            zQ(m,n)=(1/Tw)*trapz(t_int,yQ);
            n=n+1;
        end
    end

    %Averaging the PSDs for signal plus noise input
```

```matlab
            zI_avg=sum(zI)/N;
            zQ_avg=sum(zQ)/N;

            %The spectral density for signal plus noise input
            p=sqrt((zI_avg.^2)+(zQ_avg.^2));
            p1=10*log10(p);
%Comparing sensed energies with thresholds and determining 3-bit values
            n=1;
            for fk=fstart:fsweep:fstop
                if p1(n)>=T7
                    R(k,n)=7;
                elseif p1(n)>=T6
                    R(k,n)=6;
                elseif p1(n)>=T5
                    R(k,n)=5;
                elseif p1(n)>=T4
                    R(k,n)=4;
                elseif p1(n)>=T3
                    R(k,n)=3;
                elseif p1(n)>=T2
                    R(k,n)=2;
                elseif p1(n)>=T1
                    R(k,n)=1;
                else
                    R(k,n)=0;
                end
                n=n+1;
 %Note: R matrix holds the three-bit results in decimal for each node
            end
        end


%%%%%%%%%%%%%%%%%%%%%%%%%%%%%%%%%%%%%%%%%%%%%%%%%%%%%%%%%%%%%%%%%%%%%%%%%%%%
                    %THREE-BIT HARD COMBINATION
%%%%%%%%%%%%%%%%%%%%%%%%%%%%%%%%%%%%%%%%%%%%%%%%%%%%%%%%%%%%%%%%%%%%%%%%%%%%

        n=1;
        %Examining every frequency value
        for fk=fstart:fsweep:fstop
            N7=0;
            N6=0;
            N5=0;
            N4=0;
            N3=0;
            N2=0;
            N1=0;

            %Finding the number of observed energies in every region
            for k=2:M
                switch (R(k,n))
                    case 7
                        N7=N7+1;     %N7 observed energies at region 7
                    case 6
                        N6=N6+1;
                    case 5
                        N5=N5+1;
```

```
                        case 4
                            N4=N4+1;
                        case 3
                            N3=N3+1;
                        case 2
                            N2=N2+1;
                        case 1
                            N1=N1+1;
                    end
                end

                %Decision criterion
                Sum=(M-1)*N7+20*N6+5*N5+2.5*N4+1.667*N3+1.25*N2+1*N1;

                %Finding the number of detections at every frequency value
                if Sum>=M-1
                    H1(n)=H1(n)+1;   %H1 hypothesis=Signal is present
                end
                n=n+1;
            end

    end %End of 1000 times simulation run

%%%%%%%%%%%%%%%%%%%%%%%%%%%%%%%%%%%%%%%%%%%%%%%%%%%%%%%%%%%%%%%%%%%%%%%%
                %CALCULATION OF THE DETECTION PERCENTAGE
%%%%%%%%%%%%%%%%%%%%%%%%%%%%%%%%%%%%%%%%%%%%%%%%%%%%%%%%%%%%%%%%%%%%%%%%

%Below code have to be changed if sweeped frequency range or
%transmitter frequency is changed!
    Det_Perc(ss)=100*H1(33)/L;%95 MHz forms a peak at the 33rd element

end
```

B. CODE USED TO STUDY THE EFFECT OF NUMBER OF SAMPLES ON RSS-BASED LOCALIZATION

This code was used to generate the curve for five nodes in Figure 34.

```
%Volkan Sonmezer, Sep 2009, Naval Postgraduate School, Monterey,CA,USA

%This code is used to study the effect of number of samples on position
%estimation MSE of the localization part of the proposed scheme.

%All coordinates are in meter

clc
clear all
%Coordinates of the Transmitter_3
xtx3=1500;
ytx3=1100;
%EIRP of Transmitter 3 in Watts
Ptx3=1;
```

```matlab
%Coordinates of the nodes
x=[700 900 1000 300 200 1100 500 800 100 400 100 800 500 200 50  600
900 150 700 1000];
y=[250 100 200  100 300 400  450 500 550 600 50  150 200 200 300 350
400 450 500 600];

%Ideal RSS values at each node
I_RSS=[-92.02 -92 -90.38 -95.81 -95.51 -87.19 -92.3 -88.94 -95.32 -
92.47 -97.29 -92.16 -93.87 -95.97 -96.57 -92.06 -88.94 -95.27 -90 -
85.48];

%K is the coefficient representing the factors such as antenna gain and
%height that affects the RSS
%For each node, K values are equal to 1
K=1;

L=10000;      %Number of simulation runs for MSE calculation
sigma=3;      %Standard dev. of the Gaussian var. in the shadowing model
alfa=3;       %Path loss exponent
M=5;          %Number of Nodes
ss=1;

for N=100:100:1000      %Number of Samples
    for Sim=1:L             %Beginning of L simulation runs
        for k=1:M
            for m=1:N
                xi=normrnd(0,sigma);
                RSS3_0(m,k)=I_RSS(k)-0.1*xi;%Including Shadowing effect
            end
            %Numerical RSS value due to TX3 at Node k
            RSS3(k)=10^((sum(RSS3_0(:,k))/N)/10);
            A3(k,:)=[2*x(k) 2*y(k) (K/RSS3(k))^(2/alfa) -1];
            b(k,:)=[x(k)^2+y(k)^2];
        end

        %Teta3 vector gives [xtx3 ytx3 Ptx3^(2/alfa) xtx3^2+ytx3^2]
        Teta3=pinv(A3)*b;
        %Teta3=mldivide(A3,b);

        %Position Estimation Error for TX3
        E3(Sim)=sqrt((xtx3-Teta3(1))^2+(ytx3-Teta3(2))^2);

        %Absolute of transmitter EIRP estimation error for TX3
        PE3(Sim)=abs(Ptx3-Teta3(3)^(alfa/2));
    end       %End of 10000 times simulation

    %Mean Square Error for TX3
    MSE3(ss)=sum(E3')/L;
    %Average Absolute Power Estimation Error for TX3
    APEE3(ss)=sum(PE3')/L;
    ss=ss+1;
end
```

86

LIST OF REFERENCES

[1]   Ankit Mehta, T.J. Deepak, Arpit Mehta. *Compendium of Applications for Wireless Sensor Network*. [Online]. Accessed: 09/09/2009. Available: http://ankitmehta.com/Documents/whitepaper.pdf.

[2]   Michael Winkler, Klaus-Dieter Tuchs, Kester Hughes, and Graeme Barclay, "Theoretical and practical aspects of military wireless sensor networks," *Journal of Telecommunications and Information Technology*, 2/2008, pp. 37–45, 2008.

[3]   Jun Ma, Geoffrey Ye Li, and Biing Hwang (Fred) Juang, "Signal processing in cognitive radio," *Proceedings of the IEEE*, Vol. 97, No. 5, pp. 805–823, 2009.

[4]   Y. Hur, J.Park, W. Woo, K. Lim, C.-H. Lee, HS. Kim, and J. Laskar, "A wideband analog multi-resolution spectrum sensing (MRSS) technique for cognitive radio (CR) systems," *Proc. of IEEE International Symposium on Circuits and Systems*, pp. 4090–4093, 2006.

[5]   Sunghun Kim, Hyoungsuk Jeon, and Joongsoo Ma, "Robust localization with unknown transmission power for cognitive radio," *Proc. of IEEE Military Communications Conference*, pp. 1–6, 2007.

[6]   Jun Ma, Guodong Zhao, and Ye (Geoffrey) Li, "Soft combination and detection for cooperative spectrum sensing in cognitive radio networks," *IEEE Transactions on Wireless Communications*, Vol. 7, No. 11, Part2, pp. 4502–4507, 2008.

[7]   Tevfik Yücek and Hüseyin Arslan, "A survey of spectrum sensing algorithms for cognitive radio applications," *IEEE Communications Surveys and Tutorials*, Vol. 11, No. 1, pp. 116–130, 2009.

[8]   Won-Yeol Lee, Kaushik R. Chowdhury, and Mehmet C. Vuran, "Spectrum sensing algorithms for cognitive radio networks," in *Cognitive Radio Networks*, Yang Xiao and Fei Hu, eds., pp. 3–35, Auerbach Pub., Boca Raton, Florida, 2008.

[9]   S. Liu, J. Shen, R. Zhang, Z. Zhang, Y. Liu, "Information theoretic criterion based spectrum sensing for cognitive radio," *IET Communications*, Vol.2, No. 6, pp. 753–762, 2008.

[10]   Danijela Cabric and Robert W. Brodersen, "Cognitive radio spectrum sharing technology," in *Wireless Technologies, Circuits, Systems, and Devices*, Krzysztof Iniewski, ed., pp. 131–157, CRC Press, Boca Raton, Florida, 2008.

[11]   Chao Wang, Kai Liu, and Nan Xiao, "A range free localization algorithm based on restricted-area for wireless sensor networks," *Proc. of 3rd International Multi-Conference on Computing in the Global Information Technology*, pp. 97–101, 2008.

[12]   Neal Patwari, Joshua N. Ash, Spyros Kyperountas, Alfred O. Hero III, Randolph L. Moses, and Neiyer S. Correal, "Locating the nodes: cooperative localization in wireless sensor networks," *IEEE Signal Processing Magazine*, Vol. 22, No. 4, pp. 54–69, 2005.

[13]   İsmail Güvenç and Chia-Chin Chong, "A survey on TOA based wireless localization and NLOS mitigation techniques," *IEEE Communications Survey and Tutorials*, Vol. 11, No. 3, pp. 107–124, 2009.

[14]   Yun Wang, Xiaodong Wang, Demin Wang, and Dharma P. Agrawal, "Range-free localization using expected hop progress in wireless sensor networks," *IEEE Transactions on Parallel and Distributed Systems*, Vol. 20, No. 10, pp. 1540–1552, 2009.

[15]   Vijayanth Vivekanandan and Vincent W. S. Wong, "Concentric anchor beacon localization algorithm for wireless sensor networks," *IEEE Transactions on Vehicular Technology*, Vol. 56, No. 5, 2007.

[16]   J. Mitola, III, "Cognitive radio for flexible mobile multimedia communications," *Proc. IEEE Mobile Multimedia Communication Conference (MoMuC)*, pp. 3–10, New York, 1999.

[17]   Bruce Fette. *SDR Technology Implementation for the Cognitive Radio.* [Online]. Accessed: 09/09/2009. Available: ftp://ftp.fcc.gov/pub/Bureaus/Engineering_Technology/Documents/cognitive_radio/fcc_cognitive_radio_fette_v8.ppt.

[18]   Software Defined Radio Forum. *SDRF Cognitive Radio Definitions*. [Online]. Accessed: 09/09/2009. Available: http://www.sdrforum.org/pages/documentLibrary/documents/SDRF-06-R-0011-V1_0_0.pdf.

[19]   Chad M. Spooner and Richard B. Nicholls, "Spectrum sensing based on spectral correlation," in, *Cognitive Radio Technology*, 2nd Edition, Bruce Fette, ed., Burlington, Massachusetts: Academic Press, 2009.

[20]   Dian Gong, Zhiyao Ma, Yunfan Li, Wei Chen, and Zhigang Cao, "High order geometric range free localization in opportunistic cognitive sensor networks," *Proc. of IEEE International Conference on Communications Workshops*, pp. 139–143, 2008.

[21]   Curtis Scheler, *Electronic Warfare in the Information Age*. Boston: Artech House, 1999.

[22]   Qiwei Zhang, Andre B.J. Kokkeler and Gerard J.M. Smit, "An efficient multi-resolution spectrum sensing method for cognitive radio," *Proc. of Third International Conference on Communications and Networking in China*, pp.,1226–1229, 2008.

[23]   Nathan M. Neihart, Sumit Roy, and David J. Allstot, "A parallel, multi-resolution sensing technique for multiple antenna cognitive radios," *Proc. of IEEE International Symposium on Circuits and Systems*, pp. 2530–2533, 2007.

[24]   J. Park, Y. Hur, T. J. Song, K. Kim, J. Lee, K. Lim, C.-H. Lee, H. S. Kim, and J. Laskar, "Implementation issues of a wideband multi-resolution spectrum sensing (MRSS) technique for cognitive radio (CR) systems," *Proc. of 1st International Conference on Cognitive Radio Oriented Wireless Networks and Communications*, pp. 1–5, 2006.

[25]   Jongmin Park, Kwan-woo Kim, Taejoong Song, Sang Min Lee, Joonhoi Hur, Kyutae Lim, and Joy Laskar, "A cross-layer cognitive radio testbed for the evaluation of spectrum sensing receiver and interference analysis," *Proc. of 3rd International Conference on Cognitive Radio Oriented Wireless Networks and Communications,* pp. 1–6, 2008.

[26]   Amir Ghasemi, Elvino S. Sousa, "Spectrum sensing in cognitive radio networks: requirements, challenges and design trade-offs," *IEEE Communications Magazine*, Vol. 46, No. 4, pp.32–39, 2008.

[27]   Khaled Ben Letaief, and Wei Zhang, "Cooperative communications for cognitive radio networks," *Proceedings of the IEEE*, Vol. 97, No. 5, pp.878–893, 2009.

[28]   Ying-Chang Liang, Yonghong Zeng, Anh Tuan Hoang, Chee Wei Ang, and Edward Peh, "Cognitive radio for wireless regional area networks," in *Cognitive Radio Networks*, Yang Xiao and Fei Hu, eds., pp. 3–35, Auerbach Pub., Boca Raton, Florida, 2008.

[29]   Zhi Quan, Shuguang Cui, H. Vincent Poor, and Ali H. Sayed, "Collaborative wideband sensing for cognitive radios," *IEEE Signal Processing Magazine*, Vol. 25, No. 6, pp. 63–70, 2008.

[30]   Zhi Quan*,* Shuguang Cui*,* and Ali H. Sayed, "Optimal linear cooperation for spectrum sensing in cognitive radio networks," *IEEE Journal of Selected Topics in Signal Processing*, Vol. 2, No. 1, pp. 28–40, 2008.

[31]   Mourad Barkat, *Signal Detection and Estimation*, 2nd ed. Boston: Artech House, 2005.

[32]   Bernard Sklar, *Digital Communications Fundamentals and Applications*, 2nd ed. New Jersey: Prentice Hall, 2001.

[33]   Alan V. Oppenheim, Ronald W. Schafer, and John R. Buck, *Discrete-Time Signal Processing,* 2nd ed. Upper Saddle River, N.J.: Prentice-Hall, 1999.

[34]   Ralph D. Hippensteil, *Detection Theory Applications and Digital Signal Processing*. Boca Raton, Florida: CRC Press, 2002.

[35]   MATLAB Help, *Rayleigh Distribution*, Version 7.8.0.347.

[36]   Chan Chee Wei, "Distributed beamforming in wireless sensor networks," Master's thesis, Naval Postgraduate School, Monterey, California, 2004.

[37]   Owens Walker and Murali Tummala, class notes for EC4940 (Mobile Ad Hoc Wireless Networking), Naval Postgraduate School, 2009 (unpublished).

INITIAL DISTRIBUTION LIST

1. Defense Technical Information Center
   Ft. Belvoir, Virginia

2. Dudley Knox Library
   Naval Postgraduate School
   Monterey, California

3. Jeffrey B. Knorr
   Department of Electrical and Computer Engineering
   Naval Postgraduate School
   Monterey, California

4. Dan C. Boger
   Department of Information Sciences
   Naval Postgraduate School
   Monterey, California

5. Prof. Murali Tummala
   Department of Electrical and Computer Engineering
   Naval Postgraduate School
   Monterey, California

6. Prof. David Jenn
   Department of Electrical and Computer Engineering
   Naval Postgraduate School
   Monterey, California

7. Prof. Philip E. Pace
   Center for Joint Services Electronic Warfare
   Naval Postgraduate School
   Monterey, California

8. Lt. Col. Ali Basaran
   Turkish Air Force Academy
   Istanbul, Turkey

9. LCDR Mujdat Soyturk
   Turkish Naval Academy
   Istanbul, Turkey